Unradiogenic reactive phase controls the εNd of authigenic phosphates in East Antarctic margin sediment

Author(s):
Creac'h, Layla; Noble, Taryn L.; Chase, Zanna; Charlier, Bruce L.A.; Townsend, Ashley T.; Perez-Tribouillier, Habacuc; Dietz, Christian

Publication date:
2023-03-01

Permanent link:
https://doi.org/10.3929/ethz-b-000599931

Originally published in:
Geochimica et Cosmochimica Acta 344, https://doi.org/10.1016/j.gca.2023.01.001

Geochimica et Cosmochimica Acta 344 (2023) 190–206

Contents lists available at ScienceDirect

Geochimica et Cosmochimica Acta

journal homepage: www.elsevier.com/locate/gca

Unradiogenic reactive phase controls the εNd of authigenic phosphates in East Antarctic margin sediment

Layla Creac'h [a,*], Taryn L. Noble [a], Zanna Chase [a], Bruce L.A. Charlier [b], Ashley T. Townsend [c], Habacuc Perez-Tribouillier [a,d], Christian Dietz [c]

[a] Institute for Marine and Antarctic Studies, University of Tasmania, Hobart TAS, Australia
[b] Victoria University of Wellington, Wellington, New Zealand
[c] Central Science Laboratory, University of Tasmania, Hobart, TAS, Australia
[d] Laboratory of Ion Beam Physics, ETH Zürich, Switzerland

ARTICLE INFO

Article history:
Received 22 July 2022
Accepted 2 January 2023
Available online 6 January 2023
Associate editor: Franco Marcantonio

Keywords:
Neodymium isotopes
Rare Earth Elements
Leaching
Authigenic phosphate
Early diagenesis
East Antarctica

ABSTRACT

Determining past changes in ocean circulation on the Antarctic margin is important for understanding the interactions between climate, circulation, and ice sheet retreat. However, the application of neodymium isotopes (ε_{Nd}), a well-known proxy of ocean circulation, is limited on the Antarctic margin, due to the lack of carbonate preservation and inconsistency in authigenic ε_{Nd} leached from bulk sediment. Here we assess the use of the ε_{Nd} proxy along the continental rise of Wilkes Land, by combining analyses of seawater with phases extracted using a 10-second reductive leach in co-located surface sediments. Dissolved seawater ε_{Nd} values displayed the following water mass signatures; $\varepsilon_{Nd} = -8.8 \pm 0.2$ (n = 1) for Antarctic Surface Water; $\varepsilon_{Nd} = -9.7 \pm 0.2$ (n = 2) for Winter Water; and $\varepsilon_{Nd} = -8.7 \pm 0.3$ (n = 6) for modified Circumpolar Deep Water. The sediment leachate did not reproduce a bottom water Nd signature and yielded a very variable ε_{Nd}, ranging from −10.4 to −14.4. In contrast, the bulk detrital sediment ε_{Nd} fell within a narrow range of -13.1 ± 0.5 (n = 29). Examination of elemental ratios and rare earth element (REE) anomalies indicates that the leaching procedure extracts exclusively authigenic phases. The strong relationship found between phosphorus (P) and REE suggests that a P-associated phase is the main REE host-phase leached, as opposed to ferromanganese oxyhydroxides. The leached europium anomalies and ε_{Nd} indicate that the extracted Nd signature is influenced by two end members, one with a seawater-like ε_{Nd} (~-8) and one more negative than the bulk detritus (ε_{Nd} ~−14). Finally, the decoupling between [Nd] and ε_{Nd}, as well the distinct middle-REE enrichments measured in the leach implies the authigenic ε_{Nd} is controlled by diagenesis. We thus infer that the Nd signature of the leached phosphates is derived from porewater and influenced by the presence of a reactive detrital component in the sediment. Unradiogenic reactive sedimentary phases which easily dissolve into porewaters are likely sourced from the subglacial erosion of ancient metasediments and crustal remnants on the Wilkes Land coast. These new ε_{Nd} data contribute to the evaluation of the ε_{Nd} proxy at complex, dynamic and under-studied interfaces such as the East Antarctic margin. However, further work is still needed to develop reliable proxies of past Antarctic water masses.

1. Introduction

Ocean circulation plays an important role in controlling the global climate through the redistribution of heat and nutrients (Lumpkin and Speer, 2007). At the Antarctic margin, ocean circulation can affect the behaviour of the ice sheet and therefore influence global sea level (Menviel et al., 2010; Golledge et al., 2014). Modern and paleo evidence has shown that enhanced delivery of ocean heat by modified Circumpolar Deep Water (mCDW) to the Antarctic shelf drives grounding line retreat in West Antarctica (Jacobs et al., 1996; Hillenbrand et al., 2017) due to reduced ice shelf buttressing (Scambos et al., 2004). In East Antarctica, glaciers draining regions of the ice sheet grounded below sea level (e.g., Ninis, Totten, Denman, Recovery Glacier; Morlighem et al., 2020) are potentially vulnerable to ocean driven melting. The ability to trace the presence of mCDW in paleoenvironmental studies of the Antarctic margin would be a valuable tool to understand the

* Corresponding author.
E-mail address: layla.creach@utas.edu.au (L. Creac'h).

https://doi.org/10.1016/j.gca.2023.01.001
0016-7037/

links between climate, ocean circulation and ice sheet behaviour. The neodymium (Nd) isotopic composition of bottom water preserved in sedimentary archives could potentially be this tool, however the application of this proxy on the Antarctic margin is complicated (Wilson et al., 2018; Huang et al., 2020; Huang et al., 2021; Wang et al., 2022).

Neodymium is one of the rare earth elements (REE), and its isotopic ratio $^{143}Nd/^{144}Nd$ varies as a function of the initial Sm/Nd ratio of crustal material, and the time elapsed for the decay of ^{147}Sm into ^{143}Nd (i.e., the age of the rock). The oceanic Nd isotopic composition (expressed as $\varepsilon_{Nd} = [(^{143}Nd/^{144}Nd)/0.512638–1] \times 10^4$; Jacobsen and Wasserburg, 1980) is influenced by external REE inputs and water mass mixing (Elderfield et al., 1988). Since Nd has a shorter oceanic residence time (~690 years; Pöppelmeier et al., 2020b) than the global ocean mixing time (~1000 years), the dissolved ε_{Nd} has been used as a quasi-conservative tracer of ocean circulation (Piepgras and Wasserburg, 1980; Goldstein and Hemming, 2003).

Our understanding of the sources and sinks of REE to the ocean is incomplete and inconsistencies remain unresolved, such as the "Nd paradox" (Goldstein and Hemming, 2003), where dissolved Nd isotopes behave conservatively during water mass mixing but Nd concentrations exhibit a nutrient-like profile. Bertram and Elderfield, (1993) first laid out two hypotheses to explain REE and Nd isotope cycling that can be summarised as a 'top-down' control driven by dust, riverine inputs and reversible scavenging (Tachikawa et al., 2003; Arsouze et al., 2007; Siddall et al., 2008; Arsouze et al., 2009; Rempfer et al., 2011); and a 'bottom-up' control driven by boundary exchange (Lacan and Jeandel, 2005a; 2005b) and dissolved benthic flux via the sedimentary porewater system (Abbott et al., 2015a; Haley et al., 2017). The latest estimates of the oceanic Nd budget suggest that benthic fluxes dominate followed by dissolved riverine and dust inputs (Gu et al., 2019; Pöppelmeier et al., 2020b; Pasquier et al., 2022; Pöppelmeier et al., 2022). However, the exact magnitude of these fluxes, as well as the role of other sources, such as particulate riverine inputs (Rousseau et al., 2015) and ground water discharges (Johannesson and Burdige, 2007) are still unknown.

The ε_{Nd} signal of deep water masses is thought to be incorporated into sedimentary authigenic phases (Frank, 2002; Goldstein and Hemming, 2003), and has been used to reconstruct past water mass circulation (Rutberg et al., 2000; Roberts et al., 2010; Piotrowski et al., 2012; Skinner et al., 2013; Wilson et al., 2015; Williams et al., 2021). Authigenic ε_{Nd} signals have been extracted from Fe-Mn crusts or nodules (e.g., O'Nions et al., 1978; van de Flierdt et al., 2004), fish debris (e.g., Staudigel et al., 1985; Scher and Martin, 2004), foraminifera (e.g., Vance and Burton, 1999; Klevenz et al., 2008; Roberts et al., 2010) and cold-water corals (e.g., Copard et al., 2010; Struve et al., 2017). In the carbonate-free sediments of the Southern Ocean, where the availability of these archives is limited, sedimentary leaching based on the protocol of Chester and Hughes, (1967) was developed to target ferromanganese (Fe-Mn) oxyhydroxides from coatings of bulk sediment particles (Rutberg et al., 2000; Piotrowski et al., 2005) and subsequently applied in the Atlantic (Gutjahr et al., 2008; Pahnke et al., 2008; Crocket et al., 2011; Chen et al., 2012; Bohm et al., 2015; Pöppelmeier et al., 2018; Blaser et al., 2019; Pöppelmeier et al., 2020a), Indian (Gourlan et al., 2008; Wilson et al., 2013) and Pacific Oceans (Wu et al., 2015; Du et al., 2016).

Various leaching methods have been proposed in the field of paleoceanography for the extraction of Fe-Mn oxyhydroxides (Bayon et al., 2002; Gutjahr et al., 2007; Martin et al., 2010; Wilson et al., 2013; Wu et al., 2015; Blaser et al., 2016; Du et al., 2016; Huang et al., 2021). Early studies typically included a pretreatment for carbonate removal prior to acid-reductive leach (Bayon et al., 2002; Gutjahr et al., 2007), but these procedures appear to be the least reliable method, and have been avoided (Wilson et al., 2013; Molina-Kescher et al., 2014; Wu et al., 2015; Blaser et al., 2016). In recent years, the extraction of seawater derived ε_{Nd} signatures from bulk sediments has seen a move towards shorter leaching times in order to reduce the risk of extracting non-hydrogenetic phases (Wilson et al., 2013; Blaser et al., 2016; Huang et al., 2021). In some cases, however, the leached ε_{Nd} seems to be controlled by a lithogenic component, either through direct dissolution during the leaching procedure (e.g Bayon et al., 2004; Elmore et al., 2011; Kraft et al., 2013) or through an in situ control of the porewater on the authigenic ε_{Nd} (Wilson et al., 2013; Abbott et al., 2016; Du et al., 2016; Abbott et al., 2022).

The diagenetic control on the ε_{Nd} signature of authigenic Fe-Mn oxides has been shown (Palmer and Elderfield, 1985), but often overlooked in palaeoceanographic reconstructions. The ε_{Nd} signature of porewater and the importance of benthic fluxes for the REE ocean cycle has been further investigated (Abbott et al., 2015b; Abbott et al., 2015a; Haley et al., 2017), but porewater measurements remain scarce due to the complexity of porewater sampling and the large volumes required for the measurement of ε_{Nd}. Despite these challenges, Abbott et al., (2016) demonstrated the influence of porewater on the ε_{Nd} signal of authigenic phases, and a clear preferential contribution from trace mineral phases within the lithogenic component. Abbott et al., (2019) further showed that clay mineral dissolution is likely the dominant control on REE distribution of seawater, porewater and authigenic phases. Most of these studies were undertaken in the Pacific Ocean, but a recent review showed that this lithogenic control on the sedimentary authigenic ε_{Nd} records is widespread in the global ocean (Abbott et al., 2022). These findings raise concerns about the reliability of the use of authigenic ε_{Nd} as a paleo-circulation proxy. The ability of a specific leaching method to extract a seawater-derived ε_{Nd} from the bulk sediment should thus be investigated and if possible adapted on a site-by-site basis.

The few published leaching studies in the Southern Ocean reported contrasting results. Wilson et al., (2018) measured ε_{Nd} in sediment from the Wilkes subglacial basin and found that the leachate composition did not reflect a bottom water signal and co-varied with the detrital ε_{Nd}. Huang et al., (2021) proposed the use of a weak reductive leach solution, combined with a very short leaching time to extract past seawater ε_{Nd} from Southern Ocean sediments. They showed that a 10-*sec* leach provides the purest hydrogenetic signals, extracting a bottom water ε_{Nd} composition at the Filchner-Rønne Ice Shelf, in the Weddell Sea, and recovered a similar amount of Nd as when using a 30-min leach. Wang et al., (2022) found the same ε_{Nd} values using both the 10-*sec* (Huang et al., 2021) and the ~1 h leach (Blaser et al., 2016) methods in sediment from the Bellingshausen Sea. These authors did not recover a seawater ε_{Nd} composition and proposed that the dissolution of detrital particles in the studied region might control the porewater ε_{Nd}, affecting the signature of Fe-Mn oxyhydroxides during early diagenesis.

Here, we investigated the processes controlling the ε_{Nd} signature of leached sediment, and its reliability as a proxy of past bottom water circulation at the East Antarctic margin, along the continental slope of Wilkes Land. We evaluated the signal extracted from bulk sediment with the 10-*sec* leaching method of Huang et al., (2021), by comparing it directly with the ε_{Nd} of the overlying water. Additionally, we present results of trace metals and REE concentrations from the bulk, detrital and leached

sediment fractions to characterise the main REE host-phase(s) extracted from the sediment.

2. Methods

2.1. Study area and sample collection

Seawater and sediment samples were collected from the East Antarctic margin, aboard the R/V Investigator from January 14th to March 5th 2017 (IN2017_V01; Armand et al., 2018). Ten litre seawater samples were collected at 3 stations north of the Sabrina Coast (CTD-3, CTD-5, CTD-19; Fig. 1) along the continental slope. Six additional bottom water samples were collected on the continental shelf within the Dalton Polynya (DP), during another cruise aboard the Aurora Australis (AU1602 from 8th December 2016 to 21st January 2017). Samples were collected using a SBE9plus CTD rosette (Seabird Electronics) equipped with Niskin® bottles and filtered through a 0.45 µm Millipore® capsule filter directly into acid-cleaned 10 L polyethylene jerrycans. Samples were then acidified onboard to pH 2 with 2 mL/L of distilled 6 M HCl in a laminar flow hood.

CTD stations on the continental rise show seawater temperatures ranging from −1.8 to 1.4 °C and salinities from 34.0 to 34.7 psu. Results from the CTD sensors highlight three distinct water masses, previously described by Silvano et al., (2017) and Bensi et al., (2022): the Antarctic Surface Water (AASW; 0–100 m depth), the Winter Water (WW; 100–300 m) and the modified Circumpolar Deep Water (mCDW; >300 m) (Fig. 2). AASW is characterised by a potential density $\sigma_\theta < 27.55$. Below it sits WW, a colder (−1.8 °C) and slightly saltier (34.3 psu) water mass, with an 'intermediary' density ($27.55 < \sigma_\theta < 27.7$). At deeper levels, a warmer (>−0.3 °C) and saline (>34.5 psu) water mass, relatively poor in oxygen (<250 µmol.L^{-1}) can be identified as mCDW ($\sigma_\theta > 27.7$). Our sample set includes one sample of AASW (CTD 3 – 30 m), three samples of WW (CTD 3 – 150 m; CTD 5 – 139 m and CTD 19 – 124 m) and 10 samples of mCDW. The six bottom water samples collected within the Dalton Polynya reflect the composition of WW except the sample DP19 (Fig. 1), which reflects mCDW.

Surface sediment cores were collected using a multi-corer from five sites: MC01 (2161 m), MC02 (1863 m), MC03 (3099 m), MC04 (3198 m) and MC06 (3322 m) (Fig. 1).

The sample preparation and analytical procedures for Nd isotopic composition, REE and trace metal concentrations are summarized in Fig. 3 and outlined in greater detail in the following sections.

2.2. Materials and reagents

All consumables used in this study were cleaned following GEOTRACES protocols (Cutter et al., 2017). All reagents were either Baseline® ultra-high purity grade (Seastar Chemicals, Canada) and used as received (29 M hydrofluoric (HF), 12 M perchloric ($HClO_4$) acids, 11 M ammonia (NH_3) and 10 M hydrogen peroxide (H_2O_2) or distilled with a Savillex still (DST-1000) (15 M nitric (HNO_3), 11 M hydrochloric (HCl) and 18 M acetic (CH_3COOH) acids).

2.3. Seawater sample preparation

Large-volume seawater samples were pre-concentrated using pre-packed Nobias® PA1L (Hitachi Technologies, Japan) chelating resin cartridges following the method of (Pérez-Tribouillier et al., (2019). Briefly, cartridges were cleaned with 3 M HNO_3 and

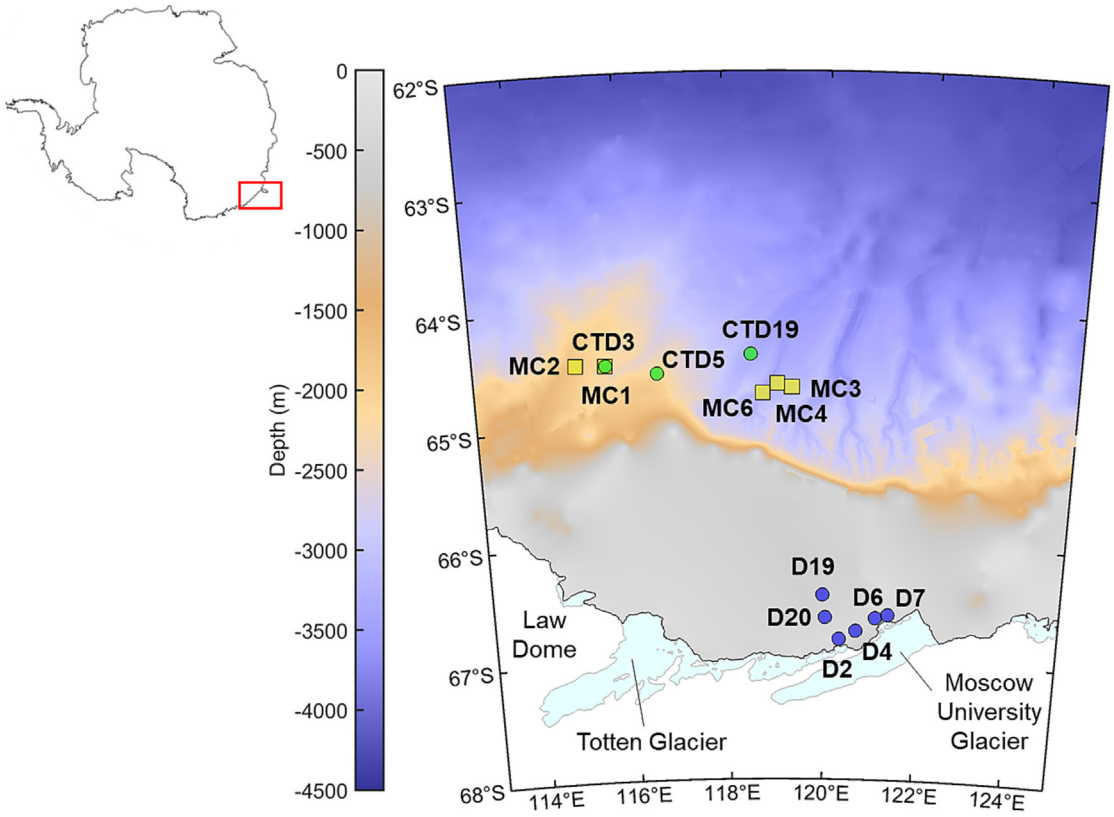

Fig. 1. High resolution bathymetry (Armand et al., 2018) of the study area and sample locations. The multi-cores ('MC'; yellow squares) and CTD seawater samples (green dots) were collected during the IN2017_V01 voyage aboard the RV Investigator; while the Dalton Polynya bottom water samples ('D'; blue dots) were collected the same year during the AU1602 voyage, aboard the Aurora Australis. Windmill Islands mentioned in the text, are located to the west of Law Dome. (For interpretation of the references to colour in this figure legend, the reader is referred to the web version of this article.)

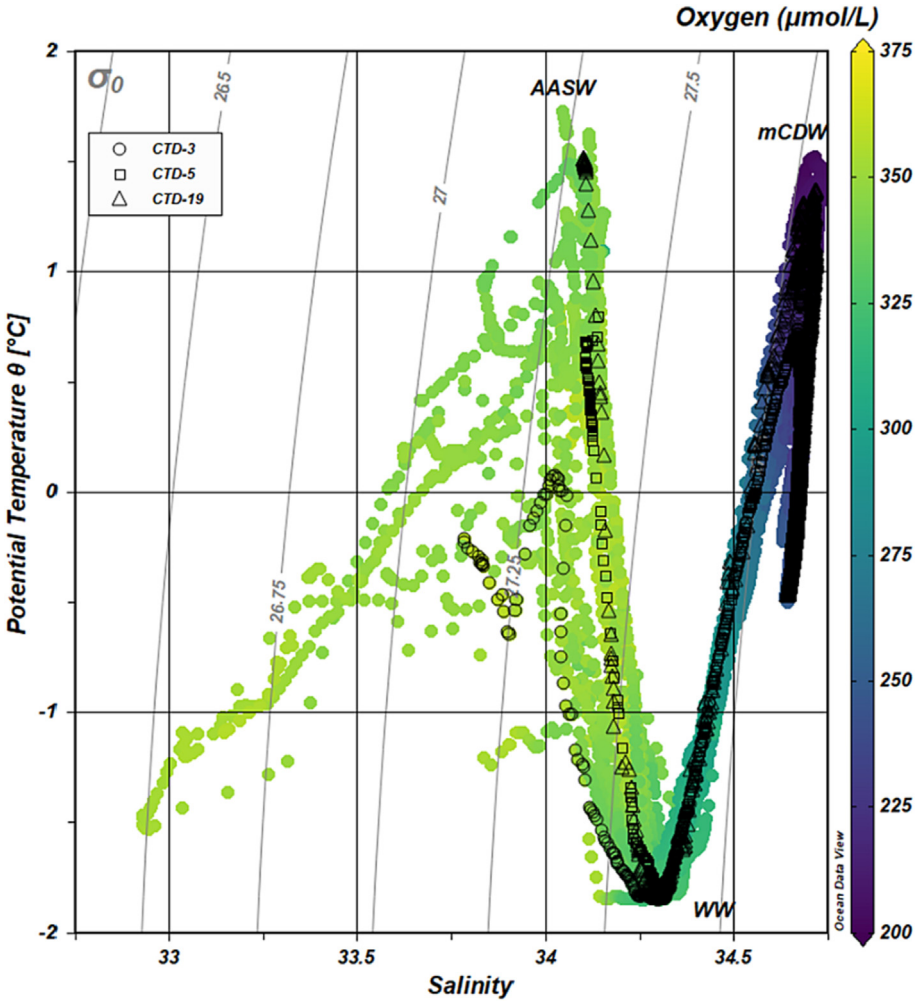

Fig. 2. Temperature-Salinity diagram for the studied CTD stations. The colour bar represents the oxygen concentration. The sampled water masses are indicated on the figure: the Antarctic Surface Water (AASW), the Winter Water (WW) and the modified Circumpolar Deep Water (mCDW). Not all seawater samples were analysed in this study but full CTD profiles are presented for easier visualisation. Figure made with Ocean Data View (ODV, Schlitzer Reiner, https://odv.awi.de).

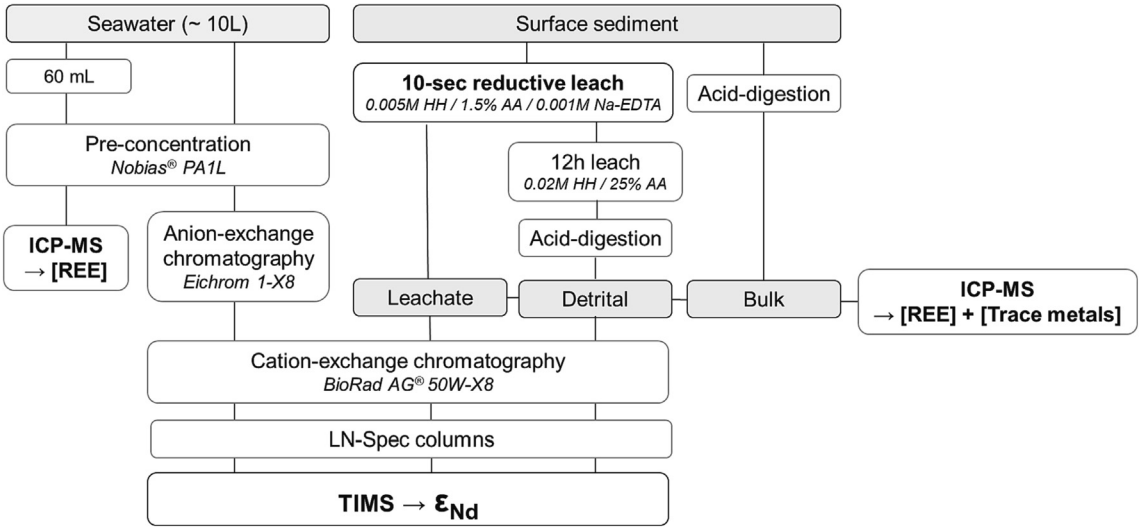

Fig. 3. Procedural schematic for the determination of ε_{Nd}, REE and trace metal concentrations in seawater, sediment leach, bulk and detrital sediment.

Milli-Q water and conditioned with 60 mL of 0.05 M ammonia acetate solution (at pH 4.75). Each sample was pH adjusted to 4.75 by adding ~210 g of 2.5 M ammonia acetate buffer solution and ~10 mL of HCl. Samples were then immediately pumped through the Nobias cartridges. The elution of Nd was achieved with 5 mL of 3.5 M HNO_3 into a Teflon vial. Pre-concentrated samples were taken to incipient dryness, oxidised, and dissolved in 1 mL HCl in preparation for ion-exchange chemistry (Fig. 3). Samples were first purified for thorium isotopes by anion-exchange chromatography (Anderson et al., 2012; results not presented here). REEs were purified via cation exchange (Struve et al., 2016), and Nd isotopes were finally isolated using LN-Spec column chemistry (Pin and Zalduegui, 1997).

Sub-samples of 60 mL seawater were preconcentrated for REE using Nobias® PA1L cartridges, following the procedure of (Hatje et al., 2014), and analysed without further purification (Fig. 3). This method provided high recovery (>80%) of dissolved REE.

2.4. Sediment dating

Twelve sediment samples from each core top (MC01-2-3-4-6) were dried, ground and submitted to Edith Cowan University (Joondalup, Western Australia) for ^{210}Pb analysis. Total ^{210}Pb, which decays into ^{210}Bi, was determined through the analysis of its granddaughter ^{210}Po by alpha spectrometry after complete sample digestion using an analytical microwave in the presence of a known amount of ^{209}Po added as a tracer (Sanchez-Cabeza et al., 1998). The concentrations of excess ^{210}Pb (Fig. 4) were determined as the difference between total ^{210}Pb and ^{226}Ra (supported ^{210}Pb), the later determined by gamma spectrometry through the measurement of its decay products ^{214}Pb and ^{214}Bi using a HPGe detector (CANBERRA, Mod. SAGe Well). The multi-cores MC01, MC03 and MC06 were then analysed for ^{14}C.

Radiocarbon dating was carried out on the bulk acid-insoluble organic carbon fraction of four samples from each core. About two grams of sediment were acidified for carbonate removal (Nieuwenhuize et al., 1994) using 2 M HCl at 85 °C. The sediment was then rinsed, dried, ground, packed into sterilised aluminium foil and sent to DirectAMS (Radiocarbon Dating Service, USA) for ^{14}C analysis.

The detection of excess ^{210}Pb ($t_{1/2}$ = 22.3 years) implies that the surface sediment is modern (<150 years old; Fig. 4), however the raw ^{14}C ages measured were excessively old (>3300 years BP) at the sediment surface (0–1 cm) and displayed reversed values at 6 and 12 cm. For this reason, only the shallowest and the deepest ^{14}C ages were used to build the age models (Table 1). The uncalibrated ^{14}C ages were corrected for "local contamination offset" (Hillenbrand et al., 2010), calculated by subtracting the core top foraminifera radiocarbon age of MC03 (Holder et al., 2020) from the raw radiocarbon age of each core top. The local reservoir age (519 ± 119 years) was estimated based on the same foraminifera radiocarbon age. Radiocarbon dates were calibrated using the *matcal* function (Lougheed and Obrochta, 2016) with the *Marine20* calibration curve (Heaton et al., 2020). The age models were then calculated using the *undatable* function with an *xfactor* of 0.1 and a *bootpc* of 10 (Lougheed and Obrochta, 2019; Supp. Mat. 1). The resulting sedimentation rates obtained for MC01, MC03 and MC06 were 7.6 cm.kyr^{-1}, 4.9 cm.kyr^{-1} and 14.7 cm.kyr^{-1} respectively.

2.5. Sediment sample preparation

2.5.1. 10-sec reductive leach

First, bulk sediment samples were dried in an oven at 40 °C. Three hundred mg of dry sediment was then homogenised and vortexed for 10-*sec* with 12 mL of a reductive solution of 0.005 M hydroxylamine hydrochloride (HH) /1.5% Acetic Acid (AA) /0.001 M Na-EDTA /0.033 M NaOH, at pH 4 (Huang et al., 2021). This reductive leaching solution was designed to target Fe-Mn oxides phases, with chelating ligand to avoid re-adsorption of leached REE onto the sediment (Gutjahr et al., 2007; Huang et al., 2021). The leach mixture was then centrifuged, and 6 mL of the supernatant solution was collected into a Teflon vial. This solution was taken to dryness, oxidized with 1 mL HNO_3 + 100 µL H_2O_2, and redissolved in 4 mL of 7.5 M HNO_3. A 0.5 mL aliquot was separated for trace metal and REE analysis. The remaining solution was taken to dryness before being taken up with 0.5 mL 3 M HNO_3 – 2.5 M HCl (3:1) for cation exchange and later LN-Spec for Nd purification (Fig. 3).

2.5.2. 12-hour leach

After the initial short 10-*sec* reductive leach, the sediment was leached a second time to ensure the removal of all oxides and excess minerals to isolate the detrital fraction (Fig. 3). Samples were leached with 15 mL of 0.02 M HH, 25% AA solution and agitated using a rotisserie (20 rpm) overnight (Wilson et al., 2018). Samples were then centrifuged, rinsed with Milli-Q water 3 times, and dried in an oven at 50 °C. About 50 mg of resulting dry (detrital) sediment was ground, weighed into a Teflon vial, and digested with a strong acid mixture (as described below).

2.5.3. Sediment digestion

Untreated bulk sediment and the operationally defined detrital fraction were weighed into a clean Teflon vial and oxidized with a mixture of concentrated HNO_3 and 30% H_2O_2 (1:1). Samples were then digested in open vials using an acid mixture comprising 10 mL HNO_3, 4 mL HCl, and 2 mL HF, at 180 °C until close to dryness. Digested residues were converted to nitric form before being oxidised with a mixture of 1 mL HNO_3 and 1 mL $HClO_4$ at 220 °C until fully desiccated. Samples were finally re-dissolved in 4 mL 7.5 M HNO3. A 400 µL aliquot was separated for trace metal and REE analysis. The remaining digest solution was taken to dryness,

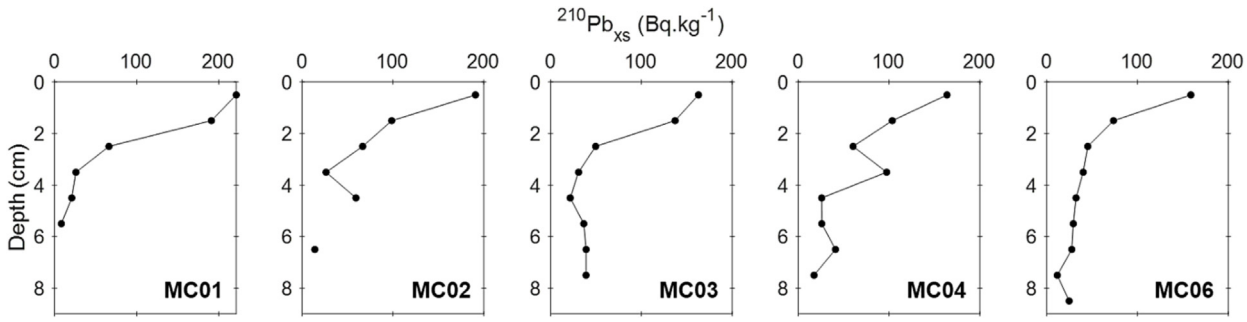

Fig. 4. Vertical profiles of excess ^{210}Pb (^{210}Pb$_{xs}$) in the multi-cores.

Table 1
Raw and calibrated radiocarbon ages measured in the multi-cores.

Core	Sediment depth *cm*	ID D-AMS	Raw ^{14}C age *years BP*	1σ	Calibrated ^{14}C age *years BP*	1σ
MC01	0–1	036871	3335	32	91	84
	19–20	036874	6315	37	2576	209
MC03	0–1	036875	5161	32	90	96
	29–29.5	036878	10,964	47	6010	191
MC06	0–1	036879	4461	32	89	79
	29–30	036882	7020	42	2065	217

oxidized, and converted to 3 M HNO_3 – 2.5 M HCl (3:1) form in preparation for Nd purification using column chemistry (Fig. 3).

2.6. Mass spectrometry

REE concentrations in seawater and sediment samples were determined using an Element 2 Sector Field Inductively Coupled Plasma Mass Spectrometer (SF-ICP-MS, Thermo Fisher Scientific, Bremen, Germany) at the Central Science Laboratory (CSL), University of Tasmania. Samples were introduced to the instrument using an Aridius® II desolvating nebulizer (CETAC Technologies, USA). The DSN was tuned daily, and oxide formation for a range of test analytes (Ba, Ce, U etc) was always <0.05%.

Relevant major and trace metals (e.g. Al, Ca, Fe, Mn, P) were analysed in sediment samples using the same SF-ICP-MS instrument, employing multiple resolution settings to minimise spectral overlap of major interferences. Samples were spiked with indium internal standard and introduced to the instrument in standard liquid aspiration mode, with quantification using the method of external calibration employing multi-elements calibration solutions (MISA suite, QCD Analysts, Spring Lake, NJ, USA).

Purified seawater and sediment sample Nd concentrations were checked using SF-ICP-MS prior to isotopic analysis. Dalton Polynya Nd isotope samples were analysed using a Neptune Plus (Thermo Scientific) with sample uptake via a CETAC Aridus 2 at the Australian National University. Nd isotope ratio measurements of all the other samples were carried out at the Geochemistry Laboratory of the School of Geography, Environment and Earth Sciences of Victoria University of Wellington, New Zealand, using a Thermo Finnigan Triton thermal ionization mass spectrometer (TIMS).

For the TIMS analyses, Nd samples were dissolved in 1 μL 2.5 M HCl, then loaded onto outgassed zone-refined double Re filaments along with 1 μL 0.25 M H_3PO_4 emitter solution. Samples were measured using filament currents of 1.2–1.4A on the evaporation side, and a temperature of 1800–1850 °C on the ionisation side of a double filament assembly. A 400 *sec* electronic baseline was measured during sample warm-up, then ratios were measured using a static collection routine consisting of 180 cycles with 10 cycles of 8.389 *sec*. each per analysis block. The cup configuration used five Faraday cups assigned to the following masses; L2 – ^{143}Nd, L1 – ^{144}Nd, C – ^{145}Nd, H1 – ^{146}Nd and H2 – ^{147}Sm. Peak centring and focussing were carried out automatically at the start of each measurement, then after every 6 blocks during the analysis. Data were reduced offline for outlier rejection and corrected using ^{146}Nd/^{144}Nd = 0.7219 (O'Nions et al., 1977) for instrumental mass fractionation using the exponential law, and ^{144}Sm/^{147}Sm = 0.20667 for the Sm interference correction on mass 144. Given the range in sample load sizes between the different sample types considered (from 2 to 108 ng Nd, with seawater samples ~24 ng Nd; leached samples ~13 ng Nd vs detrital ~95 ng Nd), two different amplifier configurations were used in order to maximise signal-to-noise ratio on the smallest samples. For the leachates, all Faraday cups were connected to $10^{13}\Omega$ resistor amplifiers, whereas the detrital samples used $10^{11}\Omega$ amplifiers (except that measuring the ^{147}Sm for the interference correction which used a $10^{13}\Omega$ amplifier). JNdi-1 standard data produced for two load sizes using both amplifier configurations were identical: ^{143}Nd/^{144}Nd = 0.512110 ± 24 2sd (46 ppm 2rsd, n = 16) for 1 ng loads using $10^{13}\Omega$ amplifiers, vs ^{143}Nd/^{144}Nd = 0.512112 ± 3 2sd (6 ppm 2rsd, n = 6) for 100 ng loads on $10^{11}\Omega$. All $10^{13}\Omega$ data were corrected for the decay constant (tau) using the Thermo Fisher proprietary software. The small offset between the measured ^{143}Nd/^{144}Nd JNdi-1 ratios and the published ^{143}Nd/^{144}Nd value of 0.512115 (Tanaka et al., 2000) was used to correct the batches of low and higher concentration samples. Dalton Polynya samples were standard bracketed with JNdi-1 at 30 ppb (^{143}Nd/^{144}Nd 0.512090; 2σ 0.000007) to 40 ppb ^{143}Nd/^{144}Nd 0.512080; 2σ 0.000014) and corrected to the accepted JNdi-1 value.

Multiple procedural blanks and certified standards (Supp. Mat. 2) were processed and analysed in the same manner as samples. The GEOTRACES intercalibration seawater BATS at 15 m (Bermuda Atlantic Time-series Study; van de Flierdt et al., 2012) and the BCR-2 standard (United States Geological Survey, USA) were used for REE analysis of seawater and sediment samples, respectively. Accuracy and precision of the seawater ε_{Nd} analysis were assessed using JNdi-1 isotopic reference material (Geological Survey of Japan, Tanaka et al., 2000); and the obtained ^{143}Nd/^{144}Nd was 0.512110 ± 0.000008 (n = 3), consistent with the published ratio of this standard.

3. Results

3.1. Seawater εNd

Over the continental rise, the sampled water masses displayed the following averaged Nd isotopic signatures: ε_{Nd} = −8.8 ± 0.2 (2σ; measurement error) for the AASW (n = 1), ε_{Nd} = −9.7 ± 0.2; n = 2 for the WW, and ε_{Nd} = −8.7 ± 0.3; n = 6 for the mCDW (Fig. 5). Only a few published ε_{Nd} values exist for AASW and WW. Our measured ε_{Nd} signatures are less radiogenic (i.e., have lower ε_{Nd} values) relative to other observations on the Antarctic margin (south of 59°S), where AASW ε_{Nd} varies from −8.3 to −5.6 in the Amundsen and Bellingshausen Sea (60-120°W; Carter et al., 2012), and has a ε_{Nd} of −8.1 ± 0.3 off the Adelie Land coast of East Antarctica (160°E; Lambelet et al., 2018). A similar AASW ε_{Nd} signature has been reported in the Indian sector (40°E; Enderby Land; −8.6 ± 0.4) by Amakawa et al., (2019), but a more radiogenic WW ε_{Nd} (−8.1 ± 0.3). To our knowledge, there are no other published data of ε_{Nd} signatures for mCDW.

On the Antarctic shelf, bottom water samples within the Dalton Polynya have the least radiogenic dissolved ε_{Nd} signatures of −10.8 ± 0.2; n = 6 (Fig. 5). These bottom water ε_{Nd} values measured on the Sabrina continental shelf correspond to some of the least radiogenic dissolved ε_{Nd} values measured around Antarctica (Basak et al., 2015; Lambelet et al., 2018; Amakawa et al., 2019).

The water column Nd concentrations measured at CTD-19 were higher than those from the western sites (CTD-3–5, Fig. 5a). This station also displayed less radiogenic water column ε_{Nd} signatures,

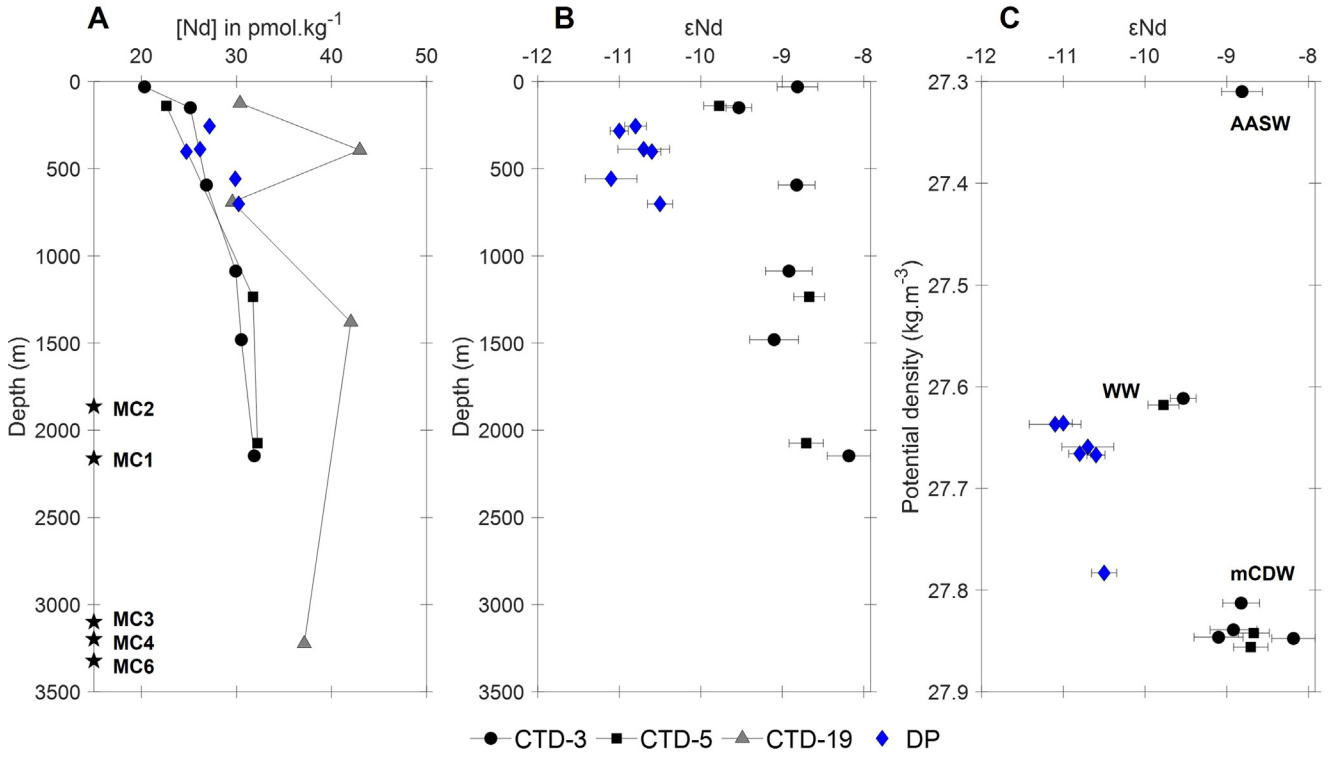

Fig. 5. (a) Dissolved Nd concentrations versus depth, (b) Nd isotopic compositions versus depth, and (c) potential density, at stations CTD-3, −5, −19 and DP. Error bars represent the 2σ measurement error. The stars on panel (a) represent the seafloor depth at which the multi-cores (MC) were collected. The sampled water masses are indicated on panel (c): the Antarctic Surface Water (AASW), the Winter Water (WW) and the modified Circumpolar Deep Water (mCDW).

with an average of ε_{Nd} = −10.2 ± 0.8; n = 4 for mCDW (not shown). We suspect issues with sample filtration for this last CTD station of the voyage, with the measurements representing a 'total' rather than dissolved fraction. The two years between sample collection and analysis may have led to the dissolution of lithogenic particles and colloids not completely filtered out. Higher concentrations of dissolved ^{232}Th (>200 pg.kg^{-1}) measured in the same samples of this station support this hypothesis. Since the aim of this study is to compare the ε_{Nd} of the leached surface sediment with the dissolved ε_{Nd} of the overlying water mass mCDW, we have removed the CTD-19 data and further discussion will focus on the mCDW signature measured at stations CTD-3 and CTD-5 (ε_{Nd} = −8.7 ± 0.3; SD; n = 6).

3.2. Sediment geochemistry

The geochemistry and phases extracted from the sediment by chemical leaching were examined through elemental analyses. Multi-core samples are made up of 70 ± 8% lithogenic (estimation based on ^{232}Th measurements), about 24 ± 5% biogenic silica, and generally no carbonate, except for the upper 0–3 cm of MC01 and MC02 (∼0.3% and 0.5% respectively; Supp. Mat. 3).

The leachate Ca/Al ratios are much higher (Ca/Al ∼ 61) than those measured in the bulk and detrital fractions (Ca/Al ∼ 0.2; Fig. 6). We note significantly higher Ca/Al in the upper bulk and leached MC01 and MC02 cores, consistent with the higher inorganic carbon (i.e., carbonate) content measured in these samples (Supp. Mat. 3). The leached Fe/Al are slightly higher (∼1.0) than in the bulk and detrital samples (∼0.6). The deepest sample of MC06 (29–30 cm) presents the lowest detrital Fe/Al. The Mn/Al and P/Al are also higher in the leachate (∼3.7 and ∼0.3) than in the bulk (∼0.02 and ∼0.01) and detrital (∼0.01 and ∼0.003) fractions.

3.3. Sedimentary εNd

The detrital sediment ε_{Nd} composition is relatively constant across samples: ε_{Nd} = −13.1 ± 0.5; n = 29 (Fig. 7a). The upper 0–10 cm detrital ε_{Nd} ranges from −12.7 to −13.6 (n = 22). The lower 15–30 cm depth ε_{Nd} composition is more variable, ranging from −10.7 to −13.9 (n = 7). In general, the detrital ε_{Nd} tends to less radiogenic values with depth, except for the deepest sample of MC06 (29–30 cm, ε_{Nd} = −10.7) where a low Fe/Al (Fig. 6) may indicate the presence of carbonate phases, rather than purely lithogenic. We hypothesise that this subsample could represent a heterogenous part of the sediment, potentially containing a shell or a fish tooth, which would explain the more radiogenic ε_{Nd} measured.

The ε_{Nd} extracted from the leached sediment is very variable, ranging from −10.4 to −14.4 (n = 28; Fig. 7b). This ε_{Nd} composition does not match the bottom seawater signal (ε_{Nd} mCDW = −8.7 ± 0.3; Fig. 5 & 7b). The variable leachate ε_{Nd} does not present a distinct trend with depth, for either the whole sample suite or within each sediment core. More than half (18/28) of the leached ε_{Nd} fall within the ε_{Nd} detrital range, while most of the remaining samples have intermediate values between detrital and seawater signatures.

3.4. Rare Earth Elements

The averaged concentrations of Nd in the different phases are: 4 ± 1 pg.g^{-1} (n = 14) in seawater, 35 ± 14 ng.g^{-1} (n = 29) in the leachate, 24 ± 3 μg.g^{-1} (n = 29) in the bulk sediment and 28 ± 5 μg.g^{-1} (n = 29) in the detrital sediment. REE element concentrations were normalised to Post-Archaean Australian Shale (PAAS; Taylor and McLennan, 1985) allowing a smooth visualisation of their chemical fractionation and highlighting any deviation from the continental

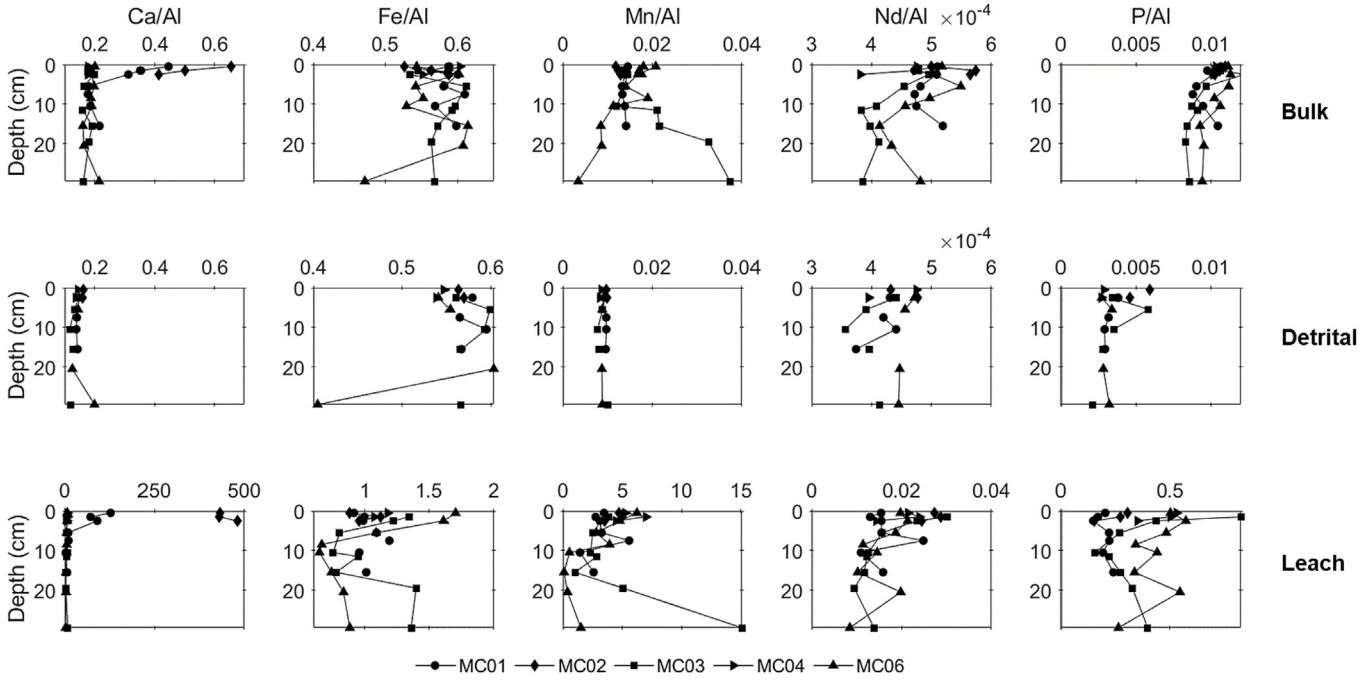

Fig. 6. Depth profiles of mass ratios Ca/Al, Fe/Al, Mn/Al, Nd/Al and P/Al in the bulk (first row), detrital (second row) and leach (third row) sediment fractions of the multicores. Note differences in ratio scales between the leachate (third row) and the bulk and detrital results.

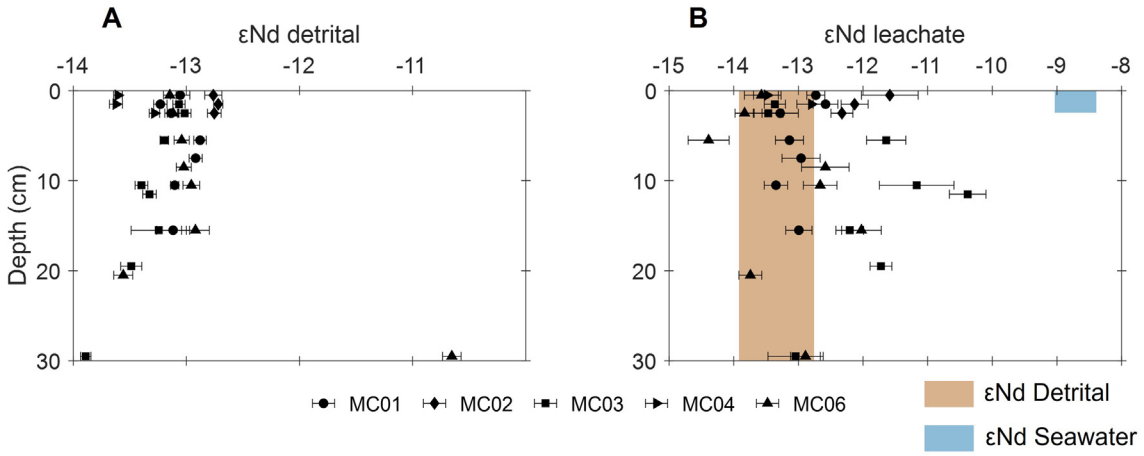

Fig. 7. ε_{Nd} measured in (a) the detrital fraction and (b) the leached sediment. The brown and blue shadings on (b) represent the range of detrital and dissolved bottom water (mCDW) ε_{Nd}, respectively. Error bars represent the 2σ measurement error. (For interpretation of the references to colour in this figure legend, the reader is referred to the web version of this article.)

crust source (Supp. Mat. 4). Averaged, minimum and maximum values are presented for easier visualisation of the data (Fig. 8).

The REE patterns display-three distinct trends (Fig. 8). The seawater PAAS-normalised REE display a typical seawater pattern, with a depletion in the light REE (LREE) relative to the heavy REE (HREE), and a negative Ce anomaly (Fig. 8a). We also observe a slightly positive Gd anomaly. In contrast, the bulk and detrital REE patterns generally present a slight enrichment in LREE (Fig. 8b & d), with positive Ce, Eu and Dy anomalies. A sharp discrepancy in these patterns is observed for the detrital sample MC06 29–30 cm (Supp. Mat. 4; Fig. S4); which again stands out because of its seawater-like HREE enrichment. This unique pattern is coherent with the more radiogenic detrital εNd signature (Fig. 7a), reflecting more authigenic components within this sample. Finally, the REE patterns of the leachates present a dominant middle REE (MREE) enrichment (MREE/MREE* > 1.3; Fig. 8c), with various anomalies depending on the sediment core. Negative Ce anomalies are observed at MC01 and MC02; whereas MC03, MC04 and MC06 present positive or no Ce anomaly (Fig. S5). Overall, the REE patterns measured in the leachate are characterised by the presence of a notable MREE bulge, significantly different from the REE patterns of the seawater and detrital fractions (Fig. 8).

4. Discussion

The sediment leachate displays a wide range of ε_{Nd} and does not record a bottom water ε_{Nd} signature (Fig. 7b). The sediment leachate ε_{Nd} values are all less radiogenic (ε_{Nd} = −10.4 to −14.4) than the Nd isotopic composition of mCDW (ε_{Nd} = −8.7), and very variable compared to the narrow detrital ε_{Nd} value (= −13.1 ± 0.5).

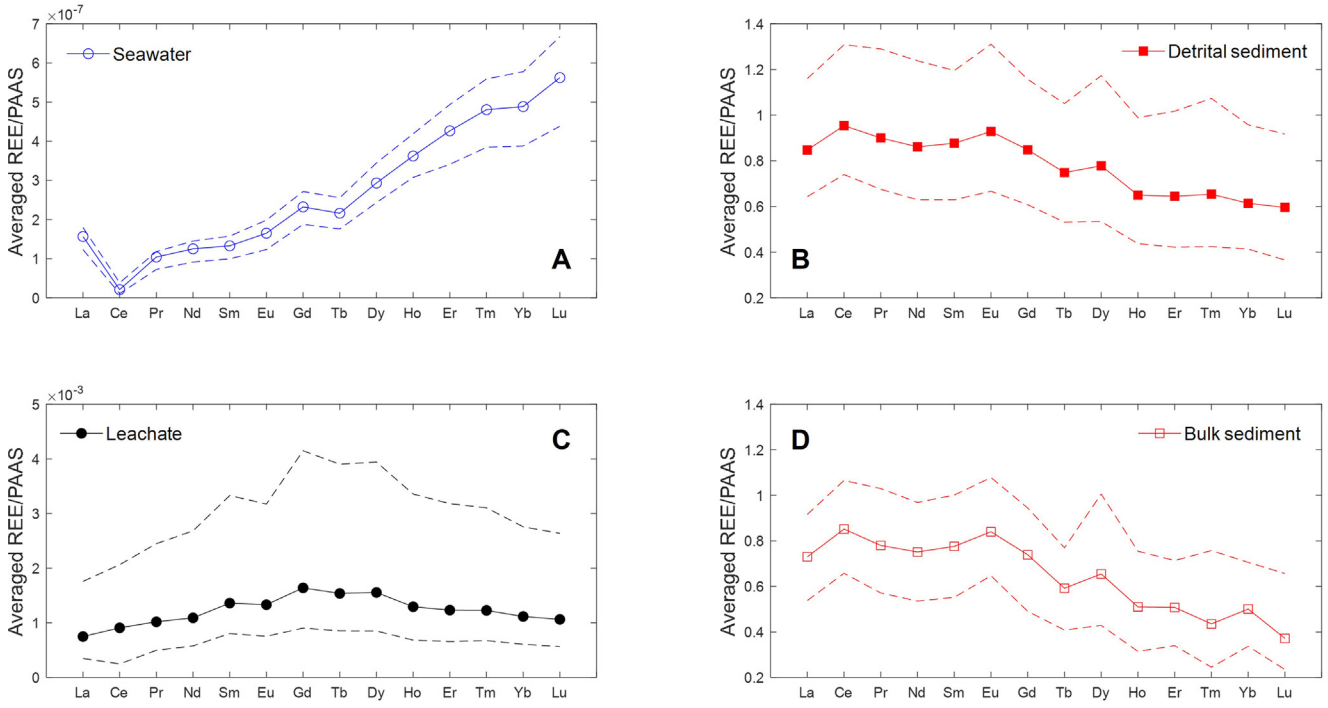

Fig. 8. Averaged PAAS-normalised REE concentrations for (a) seawater samples (n = 15), (b) detrital sediment, (c) sediment leaches, and (d) bulk sediment (n = 29). The dashed lines represent the range obtained in each phase.

The fact that the ε_{Nd} of the sediment leachates lies between the detrital and the seawater signatures (Fig. 7b) suggests we may be seeing a detrital 'contamination' of a seawater signature, with the wide range of ε_{Nd} observed representing various degrees of detrital components dissolved during the leaching procedure. However, we can rule out partial dissolution of the aluminosilicate fraction during leaching because the Al/Nd values of the leachate, which have been used to track non-hydrogenetic sources to the leach (Gutjahr et al., 2007; Blaser et al., 2016), are all very low (<100; Fig. 9a & b). The MREE enrichment (MREE/MREE* ranging from 1.3 to 1.7) observed in the sediment leachate data (Fig. 8) has been attributed to Fe-Mn oxides (Gutjahr et al., 2007) supporting the non-detrital origin of the leach. In addition, there is no correlation between the leached ε_{Nd} and the detrital ε_{Nd} (Fig. 9c). Taken together, these data suggest that the leached signature is not influenced by dissolution of the bulk detritus. Instead, we suggest that the 10-*sec* leach likely extracts an authigenic phase associated with amorphous or poorly crystalline mineral phases.

The source of the leached signature may be further investigated using the leached europium anomaly (Eu/Eu*). The leached Eu/Eu* shows a correlation (R^2 = 0.5) with the leached εNd (Fig. 10b). This relationship cannot be explained by mixing between the seawater and the bulk detrital end member (Fig. 10a). The leach data can, however, be reproduced by assuming it represents a mixture between a seawater-like endmember with an Eu/Eu* of 0.95 and a ε_{Nd} of −8.2; and an endmember representing a reactive sedimentary phase with an Eu/Eu* of 0.85 and a less radiogenic ε_{Nd} of −14.4. The resulting mixing curve (Fig. 10a) indicates that 87% of the Nd of the leach comes from this reactive phase, and 13% from the seawater-derived phase. We propose that the seawater-like endmember is derived from Fe-Mn oxides while the less radiogenic endmember represents the ε_{Nd} of a reactive sedimentary phase, distinct from the bulk detritus.

Most palaeoceanographic studies extracting REE by bulk sediment reductive HH leaching for authigenic ε_{Nd} analysis assumed that their leached ε_{Nd} was associated with the dissolution of the

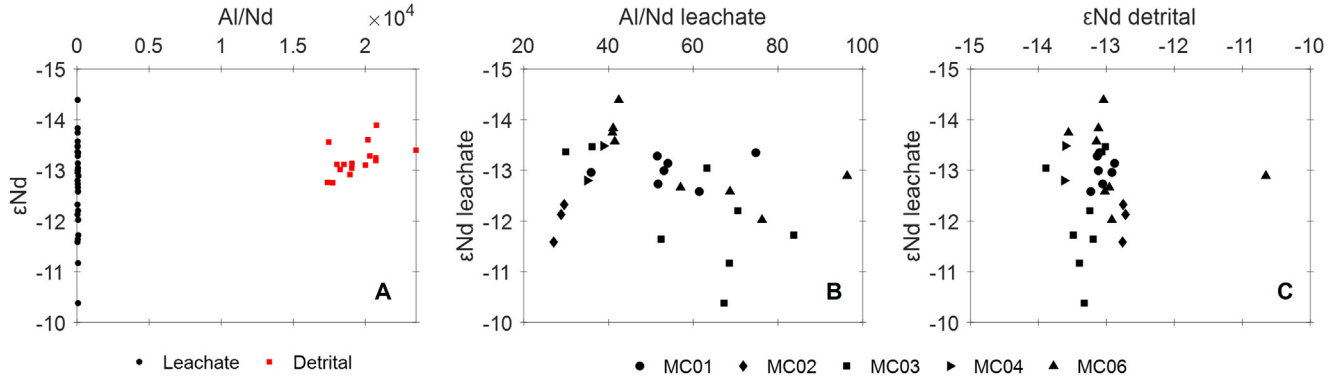

Fig. 9. (a) Al/Nd mass ratio versus ε_{Nd} measured in the leachate and in the detrital sediment fractions; (b) Al/Nd mass ratio versus ε_{Nd} measured in the leachate (R^2 = 0.10) and (c) detrital ε_{Nd} versus leached ε_{Nd}.

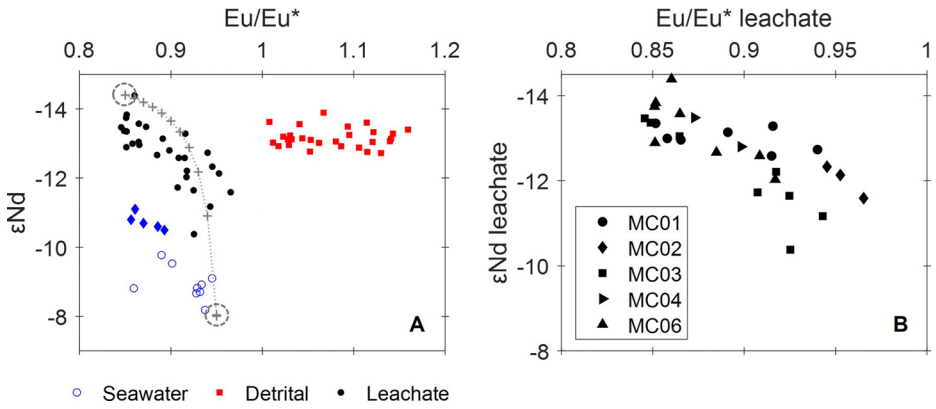

Fig. 10. (a) Eu anomaly (Eu/Eu*) versus ε_{Nd} measured in the leachate, detrital sediment and seawater. The DP bottom water samples are represented by the blue diamonds. The grey dashed line represents the mixing curve between the two assumed endmembers, selected based on the maximum and minimum data from the seawater and the leach respectively. The resulting seawater-derived endmember has a $\varepsilon_{Nd} = -8.2$ and Eu/Eu* = 0.95; and the reactive sedimentary endmember a $\varepsilon_{Nd} = -14.4$ and Eu/Eu* = 0.85. (b) Eu/Eu* versus ε_{Nd} measured in the leachate ($R^2 = 0.5$). The Eu anomalies were calculated using PAAS-normalised REE concentrations, as followed: $Eu/Eu^* = [Eu]/\overline{[Sm],[Gd]}$ (Blaser et al., 2016). (For interpretation of the references to colour in this figure legend, the reader is referred to the web version of this article.)

Fe-Mn oxyhydroxides (e.g. Rutberg et al., 2000; Piotrowski et al., 2004; Gutjahr et al., 2008; Pahnke et al., 2008; Roberts et al., 2010). However, a comparison between the geochemical signature of the leach relative to that expected for ferromanganese crusts and nodules (negative relashionship; Fig. 11; Hein and Koschinsky, 2014), suggests that authigenic Fe-Mn oxyhydroxides are not the main phases extracted on the East Antarctic margin. While elevated Fe/Al and Mn/Al in the leach indicate that Fe-Mn oxides may be present (Fig. 6), these phases are clearly not the main REE carrier phase considering the poor correlation ($R^2 = 0.4$), between [Fe] and [REE], and particularly between [Mn] and [REE] ($R^2 < 0.1$; Fig. 12a-b). This result agrees with the findings of Abbott et al., (2019), who showed that Fe-oxides are not sufficiently abundant to account for all the leached Nd in sediment from the North Pacific and the Tasman Sea; and with other studies showing that Fe cycling only plays a minor role controlling the REE distribution in sediment (Du et al., 2022) and porewater (Deng et al., 2022). The absence of correlation between [Mn] and [REE] (Fig. 12b) suggests sedimentary MnO_2 reduction and REE transfer to the porewaters.

If the leached ε_{Nd} signature is not coming from the dissolution of bulk detritus, or from the bottom water via dissolution of Fe-Mn oxyhydroxides, where is it coming from? The elemental composition of the leach suggests the presence of a phosphorus-rich phase (Fig. 6). We observed a strong positive correlation ($R^2 = 0.8$) between [P] and [REE] (Fig. 12), which suggests that reductively leachable phosphates are important REE host phases

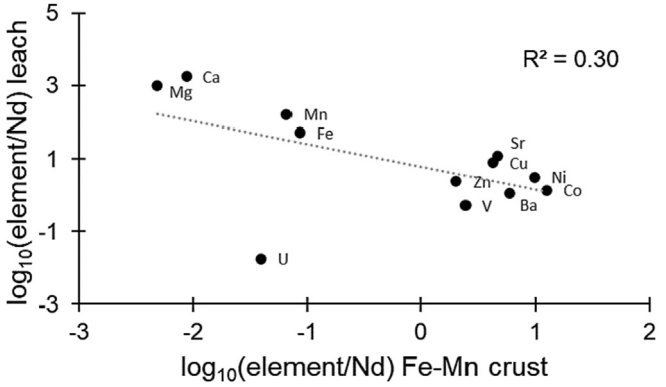

Fig. 11. Log10(element/nd) comparison between the sediment leachate and fe-mn crusts and nodules (data from Hein and Koschinsky, 2014).

in East Antarctic margin sediments. Ca-phosphates (e.g. apatite) have been proposed as a major REE carrier phase notably in sediment from the Pacific and Indian oceans (Toyoda et al., 1990; Yasukawa et al., 2014; Paul et al., 2019; Bi et al., 2021; Kim et al., 2022; Liao et al., 2022; Ren et al., 2022). Based on sequential leaching approaches for different forms of phosphate minerals in marine sediments (Ruttenberg, 1992), we suggest that the leaching solution applied liberated an exchangeable or loosely sorbed P pool, which could be associated with organic matter, reactive Fe minerals (e.g., ferrihydrite), clay minerals and P associated with Ca via carbonates or calcium phosphates (e.g., hydroxylapatite). Overall, it is hard to say with certainty which P-REE associated phase is being extracted using the single 10-*sec* leach as opposed to during sequential leaching approaches. However, considering the positive relationship ($R^2 = 0.6$) observed between the elemental composition of our leach and the composition of apatite in REE-rich mud from the Western Pacific (Fig. 13; Kon et al., 2014), authigenic apatite could be a candidate.

So far, we showed that (1) the ε_{Nd} values of the leachate do not reflect a bottom water signature, but can be explained by mixing between a seawater endmember and a reactive phase, distinct from the bulk detrital sediment (Fig. 10); and (2) the main REE-host phase extracted by the reductive leach seems to be a phosphate-phase (e.g., apatite) rather than Fe-Mn oxyhydroxides (Fig. 12). There are few possible explanations for how the leach acquires its ε_{Nd} signature. First, the leach may directly extract the ε_{Nd} signature of pre-formed phosphate minerals (Bayon et al., 2004; Kraft et al., 2013) sourced from subglacial erosion of the Wilkes Land margin, which are distinct from the bulk detrital ε_{Nd} signature. Second, the leach may extract authigenic phosphates that are formed in-situ and acquired their ε_{Nd} composition through reactive detrital phases coupled with redox processes within the sediment porewater (Wilson et al., 2013; Du et al., 2016; Abbott et al., 2019; Blaser et al., 2019; Wang et al., 2022). A third possibility is that one of the end members is pre-formed and the other formed in-situ.

The leached ε_{Nd} signature may come from 'pre-formed' authigenic phosphates, such as monazite or rhabdophane, from Wilkes Land, which would be dissolved by the leach just like hydrogenetic components precipitated directly from seawater. Monazite grains have been identified in Neoproterozoic sedimentary rocks which are interpreted to cover the Mesoproterozoic basement based on sandstone erratics collected near Windmill Islands (Maritati et al., 2019). The sparse rock outcrops of metamorphosed granites exposed in central Wilkes Land have whole rock Eu/Eu* that span

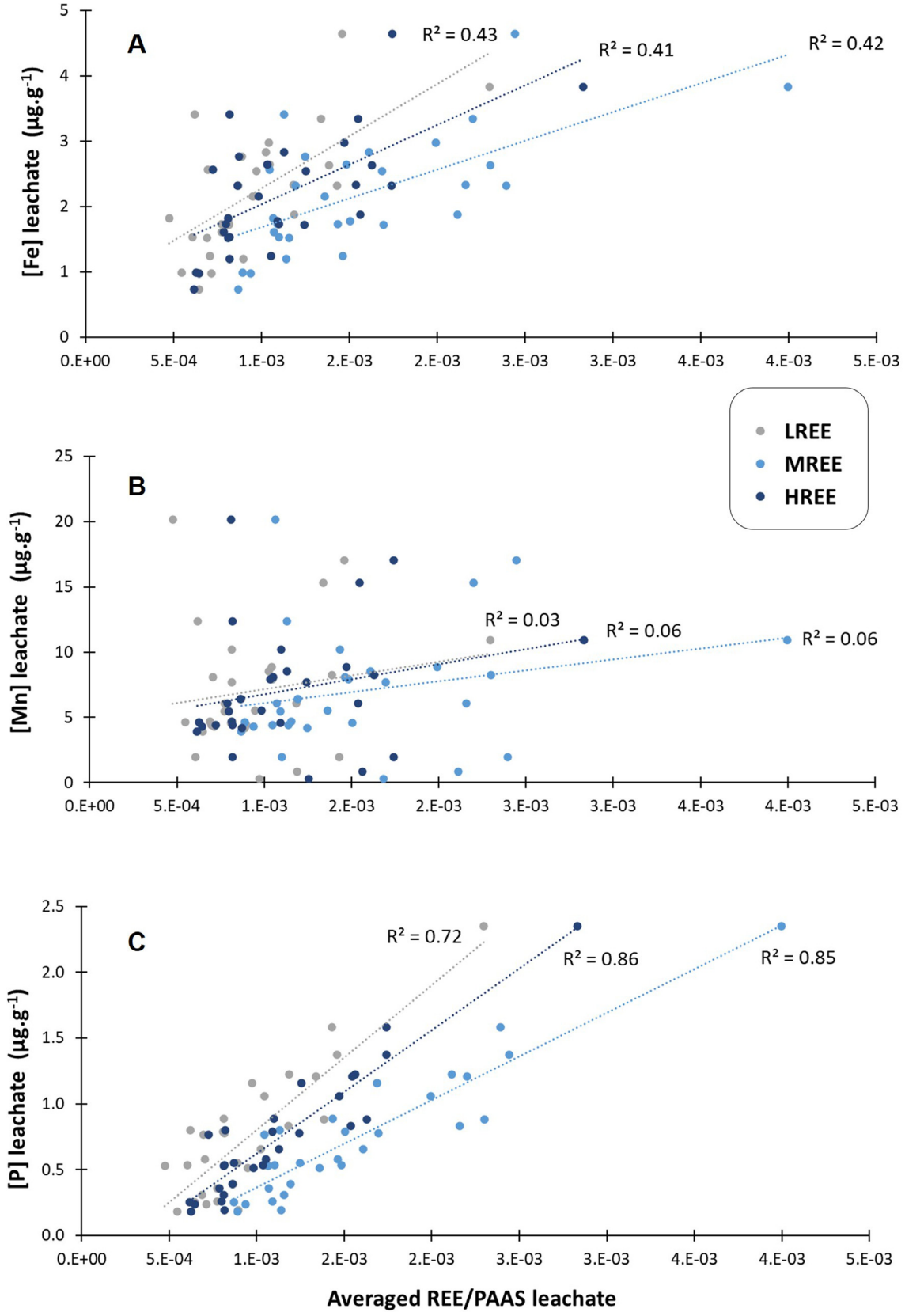

Fig. 12. Averaged (a) Fe, (b) Mn and (c) P concentrations versus PAAS-normalised REE in sediment leaches.

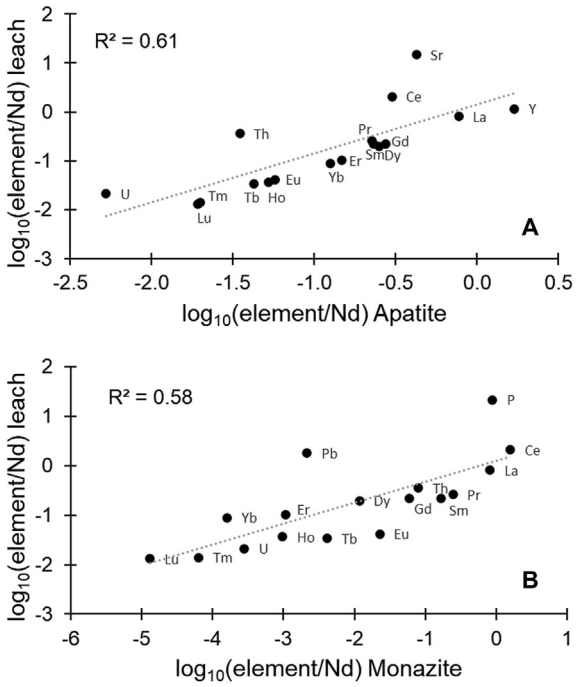

Fig. 13. Log10(element/nd) comparison between the sediment leachate and (a) apatite (data fromKon et al., 2014) and (b) monazite (data from Maritati et al., 2019).

the range observed in the leaches (0.8–1; Figs. 10 & 14), ranging from 0.4 to 3.1 (average Eu/Eu* = 1.31 (n = 13); Zhang et al., 2012; Sanchez et al., 2021). More specifically, Maritati et al., (2019) analysed authigenic monazite grains (15–50 μm) within fine grained interstitial muscovite from glacially transported sandstone erratics. These authigenic monazites match the Eu/Eu* values measured in our leaches (Fig. 14). Unfortunately, no ε_{Nd} have been measured in these monazites, but their geochemical signature normalised to [Nd] is relatively similar to the elemental ratios observed in the leach (Fig. 13). Therefore, the leached ε_{Nd} may reflect the isotopic range of pre-formed authigenic P-minerals, possibly authigenic monazite, which are being dissolved by the 10-*sec* leaching procedure.

More information on the occurrence and composition of authigenic minerals in glacial melt waters and ice rafted debris would be needed to confirm the contribution of pre-formed minerals to the geochemical signature of the leach. One line of evidence that suggests pre-formed authigenic minerals are not the main driver of the ε_{Nd} signature in the leach is the relationship between [Nd] and ε_{Nd} (Fig. 15). While the mixing curve between the seawater-derived endmember ([Nd] = 11 ng.g^{-1}; ε_{Nd} = −8.2) and the reactive sedimentary phase endmember ([Nd] = 75 ng.g^{-1}; ε_{Nd} = −14.4) broadly fits the observations, there is a lot of scatter around the line. This decoupling between ε_{Nd} and [Nd] suggests the existence of additional processes such as REE precipitation and re-scavenging possibly occurring within the sediment porewaters (Wang et al., 2022).

As an alternative to the dissolution of pre-formed authigenic phosphates, the 10-second leach may be extracting REE from phosphates that are formed in-situ and acquire their elemental

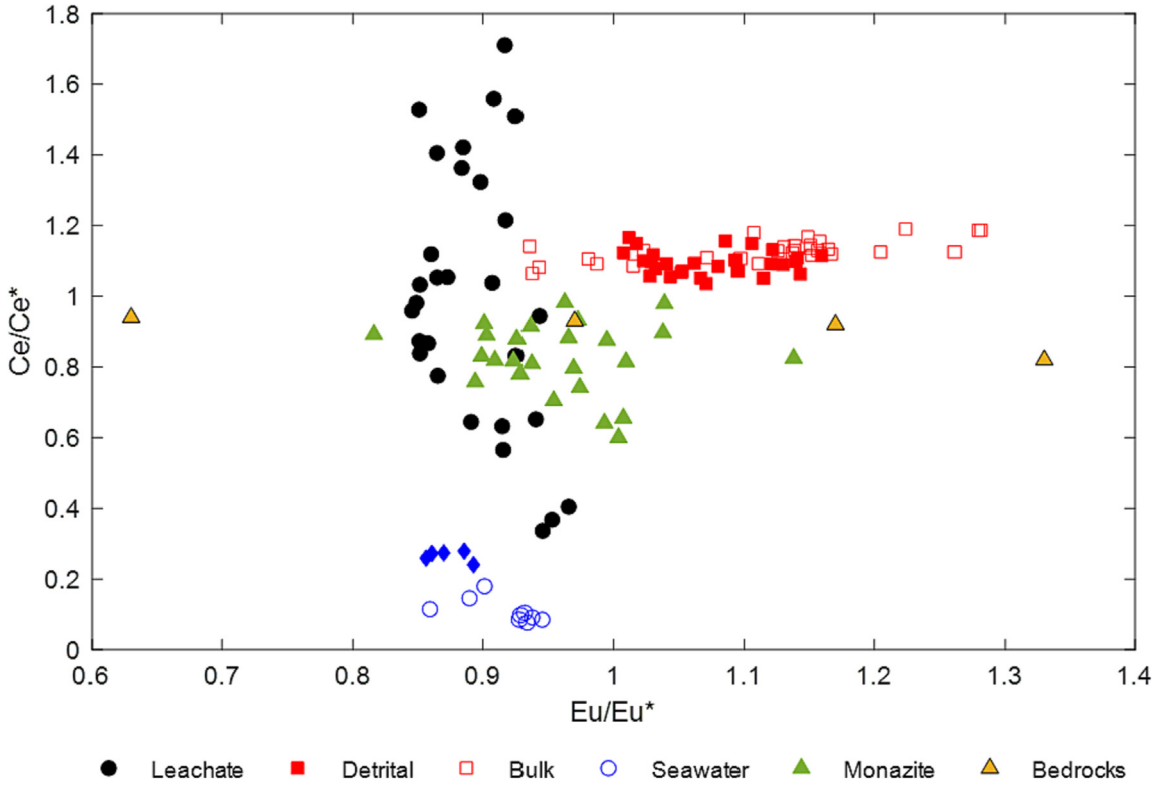

Fig. 14. Europium (Eu/Eu*) versus cerium (Ce/Ce*) anomalies in the leachate, detrital sediment, bulk sediment and seawater from the East Antarctic margin; in authigenic monazite from sandstone erratics found near Windmill Island, Wilkes Land (data from Maritati et al., 2019); and in bedrocks from Windmill Island (data from Zhang et al., 2012). The DP bottom water samples are represented by the blue diamonds. The anomalies were calculated using PAAS-normalised REE concentrations, as followed: $Eu/Eu^* = [Eu]/\overline{[Sm],[Gd]}$ and $Ce/Ce^* = [Ce]/\overline{[La],[Pr]}$ (Blaser et al., 2016). (For interpretation of the references to colour in this figure legend, the reader is referred to the web version of this article.)

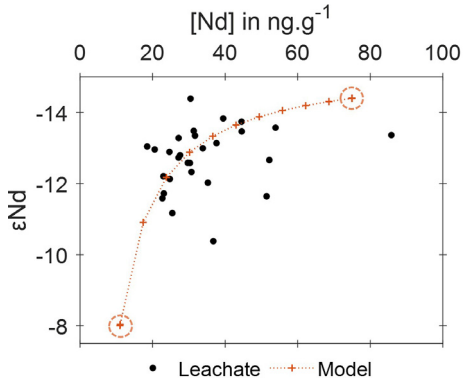

Fig. 15. Nd concentration versus ε_{Nd} measured in the leachate and modelled mixing curve. The two assumed endmembers are a seawater-derived endmember with [Nd] = 11 ng.g^{-1} and ε_{Nd} = −8.2, and a reactive detrital endmember with [Nd] = 75 ng.g^{-1} and ε_{Nd} = −14.4.

and isotopic signature via pore water exchange. There is a growing body of literature attesting to the role of porewater processes in REE cycling and impacts on leached ε_{Nd} (Abbott et al., 2016; Du et al., 2016; Abbott et al., 2019; Blaser et al., 2019; Patton et al., 2021; Abbott et al., 2022; Wang et al., 2022). We observe a MREE enrichment in all the leaches (Fig. 8), which suggests fractionation of REE associated with redox processing in the porewater (Haley et al., 2004). MREE enrichments have been attributed to the preferential release of MREE via Fe-oxide reduction (Haley et al., 2004) but also to the weathering of phosphate minerals (Hannigan and Sholkovitz, 2001).

On the West Antarctic margin Wang et al., (2022) suggested that Nd dissolved from fine-grain reactive detrital particles may get incorporated into Fe-Mn oxyhydroxides via porewater exchange. A similar mechanism of REE incorporation into authigenic phosphates (instead of Fe-Mn oxyhydroxides) could explain the ε_{Nd} signatures observed in our leachate. Indeed, it has been shown that the REE budget of authigenic apatite is mostly derived from porewater rather than seawater (Toyoda and Tokonami, 1990; Chen et al., 2015; Trotter et al., 2016; Paul et al., 2019). Additionally, it has been shown that Mn-oxides transfer their REE to phosphates during early diagenesis (Takahashi et al., 2015), which could explain why the P-associated phase seems to carry a larger proportion of REE compared to Mn oxides (Fig. 12). This explanation agrees with the model simulation of Du et al., (2022) which found that MnO_2 reduction is the main source of Nd in porewater, while phosphate precipitation is the main sink. We thus suggest that the seawater-like endmember is derived from Mn oxides that initially host the seawater-sourced REE, which are then transferred to the porewater through reduction during early diagenesis. We further propose that the less radiogenic endmember is a reactive minor component of the detritus, which is also transferred to porewater during early diagenesis (Fig. 16). Zhang et al., (2012) and Möller et al., (2002) reported the presence of ancient (Paleoarchean) metasedimentary crustal remnants at Windmill Islands with very low ε_{Nd} values of −18.1 and −26.1 respectively, which are sufficiently 'unradiogenic' to represent the isotopic composition of our reactive sedimentary end member (ε_{Nd} = 14.4; (Fig. 10a) affecting the ε_{Nd} composition of the leach. This is consistent with other studies suggesting that the signature of the reactive detrital particles may have more extreme ε_{Nd} than the detrital sediment itself (Abbott et al., 2016; Du et al., 2016; Wilson et al., 2013; Wu et al., 2015). The presence of such reactive phases is expected in this setting; sediments on the Antarctic margin contain minerals that have undergone extensive physical but limited chemical weathering, similar to what has been observed in the Labrador Sea (Howe et al., 2016), supplying reactive mineral components with large surface areas that readily dissolve or exchange cations within the porewater.

We suggest that the same process, that is early diagenesis, occurs within the continental shelf sediments above the Dalton Polynya and shifts the bottom waters from ε_{Nd} = −8.7 values to ~−11 (Fig. 5). The unradiogenic source of ε_{Nd} released by the reactive sedimentary phase into the porewaters on the continental shelf is likely more pronounced than on the continental rise due to the high productivity occurring in the polynya (Moreau et al., 2019), which would result in more reducing conditions; but also due to the closer proximity to the source of chemically reactive, freshly eroded, fine glaciogenic sediment. However, ε_{Nd} measurements of porewaters or leached ε_{Nd} from the shelf sediments would be required to explore these processes.

Further work investigating the origin of this trace reactive detrital phase and isotopic values of outcrops and erratics from Wilkes Land would be useful for understanding their control on the ε_{Nd} signatures of sedimentary porewater and authigenic records. The correlation between Eu/Eu* and ε_{Nd} (Fig. 10) suggests that the Eu anomaly might be a good proxy allowing to identify the source of these reactive phases, assuming that Eu/Eu* is preserved through the processes of dissolution in porewater and incorporation into authigenic phases. The measurement of Eu/Eu* combined with mineralogy of the sample might thus help to identify the reactive detrital components present in the studied sediment. However, this may not be possible since trace reactive components are not easily separable from the bulk sediment, and often have concentrations below detection limit for other analyses (e.g., XRD; Ruttenberg and Berner, 1993; Abbott et al., 2019). Overall, complementary tests should also be undertaken in sediment cores collected further away from the Antarctic margin, as well as more porewater analyses.

To sum up, we suggest that the wide range of ε_{Nd} measured in the leaches (Fig. 7) and the observed decoupling between [Nd] and ε_{Nd} (Fig. 15) can be best explained by partial dissolution of a reactive detrital component and porewater exchange with authigenic

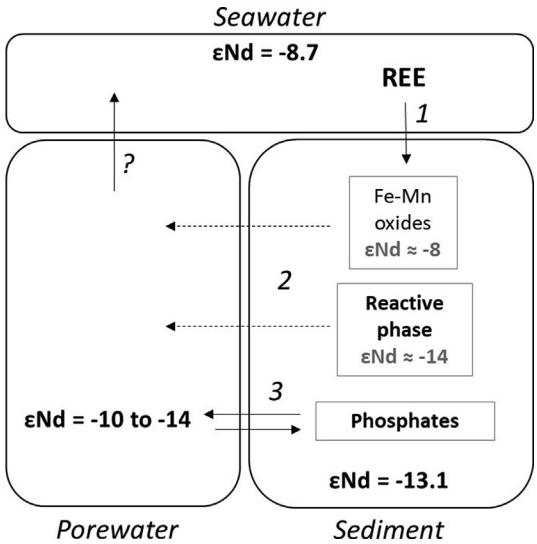

Fig. 16. Conceptual diagram to explain the origin of ε_{Nd} to the authigenic phase within East Antarctic margin sediment. (1) REE inputs to the sediment pile; (2) Partial dissolution of Fe-Mn oxides and trace reactive phase, with ε_{Nd} transfer into the porewater; (3) ε_{Nd} incorporation into authigenic phosphate via porewater exchanges. The ε_{Nd} in black are measured signatures and the ones in grey are assumed endmembers modelled by the mixing curve in Fig. 10. We assume that the ε_{Nd} of the sediment leachate (extracting leachable phosphates) reflects the porewater ε_{Nd} signature. For details and references, refer to the main text.

phases formed in-situ (Wilson et al., 2013; Du et al., 2016; Abbott et al., 2022; Wang et al., 2022). We propose the following processes occur at the East Antarctic margin (Fig. 16): (1) inputs of REE via Fe-Mn oxides, organic matter and lithogenic particles into the sediment pile (Sholkovitz et al., 1994; Schijf et al., 2015); (2) partial dissolution of a trace reactive detrital component, Fe-Mn oxide reduction and transfer of ε_{Nd} signatures into the porewater (Abbott et al., 2016; Du et al., 2016; Abbott et al., 2019; Abbott et al., 2022; Du et al., 2022); (3) P precipitation (authigenic mineral formation; Byrne and Kim, 1993) and diagenetic incorporation of the ε_{Nd} signatures into authigenic phosphates (Takahashi et al., 2015; Bi et al., 2021; Du et al., 2022); (4) REE re-scavenging responsible for the decoupling between the ε_{Nd} and [Nd] in the leach (Wang et al., 2022).

The 10-*sec* leach is a suitable method to extract authigenic phases from Southern Ocean sediment but the authigenic record does not preserve the seawater ε_{Nd} signatures from sediments on the Wilkes Land margin. The ability of reductive leaches to extract a bottom water ε_{Nd} is highly dependent on the location. Huang et al., (2021) obtained leached sediment ε_{Nd} matching bottom water ε_{Nd} in the Weddell Sea. However, this study, as well as Wang et al., (2022) showed that reactive detrital components can prevent the extraction of a seawater ε_{Nd} signal at the East and West Antarctic margins respectively. In some locations, it may be that the reactive detrital component matches the bottom water ε_{Nd} (Patton et al., 2021). A better understanding of interactions between bottom water, pore water and authigenic and detrital sediment phases is essential to evaluate the reliability of existing proxies, and to develop and improve the calibration of new ones. Finally, our results confirm the importance of undertaking this type of study before carrying out palaeoceanographic reconstructions.

5. Conclusions

We tested the application of sedimentary authigenic ε_{Nd} as a proxy of paleo-circulation on the East Antarctic margin. We applied a short 10-second leaching procedure (Huang et al., 2021) in surface sediment, and compared the ε_{Nd} in the leach with the ε_{Nd} of the overlying bottom water. The εNd measured in the leach did not match the seawater signal, preventing its use as a paleo-circulation proxy in this region. The leach and sedimentary elemental ratios and REE results show that the leaching procedure extracts an authigenic phase with REEs predominantly associated with a phosphate-phase (possibly apatite and/or monazite). We suggest that the leached ε_{Nd} is influenced by a seawater-derived signal which is overprinted by a trace, reactive and isotopically distinct component present within the sediment, that transfers its ε_{Nd} to the authigenic phase through porewater processes. This study confirms the importance of phosphates as sedimentary REE carrier-phases and the dominance of diagenetic processes for the control of the signature of authigenic ε_{Nd}. Further work is needed to develop proxies of paleo-circulation around Antarctica.

Declaration of Competing Interest

The authors declare that they have no known competing financial interests or personal relationships that could have appeared to influence the work reported in this paper.

Acknowledgements

We would like to acknowledge the crew and captain of the RV Investigator, as well as the chief scientists Leanne Armand and Philip O'Brien for their support during the IN2017_V01 voyage. We thank Delphine Lannuzel and Matthew Corkill for the seawater sample collection during the AU1602 voyage. We also thank Pere Masqué for the multi-core ^{210}Pb analyses. We are grateful to Pam Quayle and Axel Durand for their help and support in the lab; to Matthew Corkill for his assistance with MATLAB and to Patrick Blaser for helpful discussions. We are grateful to Martin Frank for sharing seawater from BATS to assess the accuracy of our seawater REE method. Finally, we would like to thank the two reviewers for their valuable constructive comments which significantly improved this manuscript.

This project was funded by the Australian Antarctic Program Project 4419, with access to ICP instrumentation supported through ARC LIEF funds (LE0989539). ^{210}Pb analyses were funded through an ARC LIEF project (LE170100219). The PhD scholarship of L.C. was provided by the University of Tasmania.

Appendix A. Supplementary material

Research data associated with this article can be access at the Australian Antarctic Data repository: ^{210}Pb (https://doi.org/10.26179/xtg1-9t49); ^{14}C (https://doi.org/10.26179/fc8h-6z85); Total and organic carbon concentrations (https://doi.org/10.26179/j699-g209); Trace metals concentrations measured in the bulk sediment (https://doi.org/10.26179/50pv-w074), in the detrital sediment (https://doi.org/10.26179/vnv3-gf49) and in the sediment leachate (https://doi.org/10.26179/p7nn-w677); Nd isotopic composition (εNd) measured in seawater (https://doi.org/10.26179/yf2t-ac49), in the detrital sediment (https://doi.org/10.26179/aqn5-6171), and in the sediment leachate (https://doi.org/10.26179/y9az-xs50); Rare Earth Elements concentrations measured in seawater (https://doi.org/10.26179/xftj-vg21), in the bulk sediment (https://doi.org/10.26179/m11r-q560), in the detrital sediment (https://doi.org/10.26179/vn9p-bz20) and in the sediment leachate (https://doi.org/10.26179/qgd3-qc54).

Supplementary material to this article can be found online at https://doi.org/10.1016/j.gca.2023.01.001.

References

Abbott, A.N., Haley, B.A., McManus, J., 2015a. Bottoms up: Sedimentary control of the deep North Pacific Ocean's εNd signature. Geology 43, 1035–1038.

Abbott, A.N., Haley, B.A., Mcmanus, J., Reimers, C.E., 2015b. The sedimentary flux of dissolved rare earth elements to the ocean. Geochim. Cosmochim. Acta 154, 186–200.

Abbott, A.N., Haley, B.A., McManus, J., 2016. The impact of sedimentary coatings on the diagenetic Nd flux. Earth Planet. Sci. Lett. 449, 217–227.

Abbott, A.N., Löhr, S., Trethewy, M., 2019. Are clay minerals the primary control on the oceanic rare earth element budget? Front. Mar. Sci. 6, 504.

Abbott, A.N., Löhr, S.C., Payne, A., Kumar, H., Du, J., 2022. Widespread lithogenic control of marine authigenic neodymium isotope records? Implications for paleoceanographic reconstructions. Geochim. Cosmochim. Acta 319, 318–336.

Amakawa, H., Yu, T.L., Tazoe, H., Obata, H., Gamo, T., Sano, Y., Shen, C.C., Suzuki, K., 2019. Neodymium concentration and isotopic composition distributions in the southwestern Indian Ocean and the Indian sector of the Southern Ocean. Chem. Geol. 511, 190–203.

Anderson, R.F., Fleisher, M.Q., Robinson, L.F., Edwards, R.L., Hoff, J.A., Moran, S.B., van der Loeff, M.R., Thomas, A.L., Roy-Barman, M., Francois, R., 2012. GEOTRACES intercalibration of 230Th, 232Th, 231Pa, and prospects for 10Be. Limnol. Oceanogr. Methods 10, 179–213.

Armand L. K., O'Brien P. E., Armbrecht L., Baker H., Caburlotto A., Connell T., Cotterle D., Duffy M., Edwards S., Evangelinos D., Fazey J., Flint A., Forcardi A., Gifford S., Holder L., Hughes P., Lawler K.-A., Lieser J., Leventer A., Lewis M., Martin T., Morgan N., López-Quirós A., Malakoff K., Noble T., Opdyke B., Palmer R., Perera R., Pirotta V., Post A., Romeo R., Simmons J., Thost D., Tynan S. and Young A. (2018) Interactions of the Totten Glacier with the Southern Ocean through multiple glacial cycles (IN2017-V01): Post-survey report. ANU Res. Publ.

Arsouze, T., Dutay, J.C., Lacan, F., Jeandel, C., 2007. Modeling the neodymium isotopic composition with a global ocean circulation model. Chem. Geol. 239, 165–177.

Arsouze, T., Dutay, J.C., Lacan, F., Jeandel, C., 2009. Reconstructing the Nd oceanic cycle using a coupled dynamical - biogeochemical model. Biogeosciences 6, 2829–2846.

Basak, C., Pahnke, K., Frank, M., Lamy, F., Gersonde, R., 2015. Neodymium isotopic characterization of Ross Sea Bottom Water and its advection through the southern South Pacific. Earth Planet. Sci. Lett. 419, 211–221.

Bayon, G., German, C.R., Boella, R.M., Milton, J.A., Taylor, R.N., Nesbitt, R.W., 2002. An improved method for extracting marine sediment fractions and its application to Sr and Nd isotopic analysis. Chem. Geol. 187, 179–199.
Bayon, G., German, C.R., Burton, K.W., Nesbitt, R.W., Rogers, N., 2004. Sedimentary Fe-Mn oxyhydroxides as paleoceanographic archives and the role of aeolian flux in regulating oceanic dissolved REE. Earth Planet. Sci. Lett. 224, 477–492.
Bensi, M., Kovačević, V., Donda, F., O'Brien, P.E., Armbrecht, L., Armand, L.K., 2022. Water masses distribution offshore the Sabrina Coast (East Antarctica). Earth Syst. Sci. Data 14, 65–78.
Bertram, C.J., Elderfield, H., 1993. The geochemical balance of the rare earth elements and neodymium isotopes in the oceans. Geochim. Cosmochim. Acta 57, 1957–1986.
Bi, D., Shi, X., Huang, M., Yu, M., Zhou, T., Zhang, Y., Zhu, A., Shi, M., Fang, X., 2021. Geochemical and mineralogical characteristics of deep-sea sediments from the western North Pacific Ocean: Constraints on the enrichment processes of rare earth elements. Ore Geol. Rev. 138, 104318.
Blaser, P., Lippold, J., Gutjahr, M., Frank, N., Link, J.M., Frank, M., 2016. Extracting foraminiferal seawater Nd isotope signatures from bulk deep sea sediment by chemical leaching. Chem. Geol. 439, 189–204.
Blaser, P., Pöppelmeier, F., Schulz, H., Gutjahr, M., Frank, M., Lippold, J., Heinrich, H., Link, J.M., Hoffmann, J., Szidat, S., Frank, N., 2019. The resilience and sensitivity of Northeast Atlantic deep water εNd to overprinting by detrital fluxes over the past 30,000 years. Geochim. Cosmochim. Acta 245, 79–97.
Bohm, E., Lippold, J., Gutjahr, M., Frank, M., Blaser, P., Antz, B., Fohlmeister, J., Frank, N., Andersen, M.B., Deininger, M., 2015. Strong and deep Atlantic meridional overturning circulation during the last glacial cycle. Nature 517, 73–76.
Byrne, R.H., Kim, K.H., 1993. Rare earth precipitation and coprecipitation behavior: The limiting role of PO43- on dissolved rare earth concentrations in seawater. Geochim. Cosmochim. Acta 57, 519–526.
Carter, P., Vance, D., Hillenbrand, C.D., Smith, J.A., Shoosmith, D.R., 2012. The neodymium isotopic composition of waters masses in the eastern Pacific sector of the Southern Ocean. Geochim. Cosmochim. Acta 79, 41–59.
Chen, J., Algeo, T.J., Zhao, L., Chen, Z.Q., Cao, L., Zhang, L., Li, Y., 2015. Diagenetic uptake of rare earth elements by bioapatite, with an example from Lower Triassic conodonts of South China. Earth-Sci. Rev. 149, 181–202.
Chen, T.Y., Frank, M., Haley, B.A., Gutjahr, M., Spielhagen, R.F., 2012. Variations of North Atlantic inflow to the central Arctic Ocean over the last 14 million years inferred from hafnium and neodymium isotopes. Earth Planet. Sci. Lett. 353–354, 82–92.
Chester, R., Hughes, M.J., 1967. A chemical technique for the separation of ferro-manganese minerals and adsorbed trace elements from pelagic sediments. Chem. Geol. 2, 249–262.
Copard, K., Colin, C., Douville, E., Freiwald, A., Gudmundsson, G., De Mol, B., Frank, N., 2010. Nd isotopes in deep-sea corals in the North-eastern Atlantic. Quat. Sci. Rev. 29, 2499–2508.
Crocket, K.C., Vance, D., Gutjahr, M., Foster, G.L., Richards, D.A., 2011. Persistent Nordic deep-water overflow to the glacial North Atlantic. Geology 39, 515–518.
Cutter, G., Casciotti, K., Croot, P., Geibert, W., Heimbürger, L.-E., Lohan, M., Planquette, H., van de Flierdt, T., 2017. Sampling and Sample-handling Protocols for GEOTRACES Cruises.
Deng, K., Yang, S., Du, J., Lian, E., Vance, D., 2022. Dominance of benthic flux of REEs on continental shelves: implications for oceanic budgets. Geochem. Perspect. Lett. 22, 26–30.
Du, J., Haley, B.A., Mix, A.C., 2016. Neodymium isotopes in authigenic phases, bottom waters and detrital sediments in the Gulf of Alaska and their implications for paleo-circulation reconstruction. Geochim. Cosmochim. Acta 193, 14–35.
Du, J., Haley, B.A., Mix, A.C., Abbott, A.N., McManus, J., Vance, D., 2022. Reactive-transport modeling of neodymium and its radiogenic isotope in deep-sea sediments: The roles of authigenesis, marine silicate weathering and reverse weathering. Earth Planet. Sci. Lett. 596, 117792.
Elderfield, H., Whitfield, M., Burton, J.D., Bacon, M.P., Liss, P.S., 1988. The oceanic chemistry of the rare-earth elements [and Discussion]. Philos. Trans. R. Soc. Lond. Ser. A Math. Phys. Sci. 325, 105–126.
Elmore, A.C., Piotrowski, A.M., Wright, J.D., Scrivner, A.E., 2011. Testing the extraction of past seawater Nd isotopic composition from North Atlantic deep sea sediments and foraminifera. Geochem. Geophys. Geosyst. 12, 1–13.
Frank, M., 2002. Radiogenic isotopes: tracers of past ocean circulation and erosional input. Rev. Geophys. 10, 1–38.
Goldstein, S.L., Hemming, S.R., 2003. Long-lived Isotopic Tracers in Oceanography, Paleoceanography and Ice Sheet Dynamics. Treat. Geochem. 6, 625.
Golledge, N.R., Menviel, L., Carter, L., Fogwill, C.J., England, M.H., Cortese, G., Levy, R. H., 2014. Antarctic contribution to meltwater pulse 1A from reduced Southern Ocean overturning. Nat. Commun. 5, 5107.
Gourlan, A.T., Meynadier, L., Allègre, C.J., 2008. Tectonically driven changes in the Indian Ocean circulation over the last 25 Ma: Neodymium isotope evidence. Earth Planet. Sci. Lett. 267, 353–364.
Gu, S., Liu, Z., Jahn, A., Rempfer, J., Zhang, J., Joos, F., 2019. Modeling Neodymium Isotopes in the Ocean Component of the Community Earth System Model (CESM1). J. Adv. Model. Earth Syst. 11, 624–640.
Gutjahr, M., Frank, M., Stirling, C.H., Klemm, V., Flierdt, T., De, V., Halliday, A. N., 2007. Reliable extraction of a deepwater trace metal isotope signal from Fe–Mn oxyhydroxide coatings of marine sediments. Chemical 242, 351–370.
Gutjahr, M., Frank, M., Stirling, C.H., Keigwin, L.D., Halliday, A.N., 2008. Tracing the Nd isotope evolution of North Atlantic Deep and Intermediate Waters in the western North Atlantic since the Last Glacial Maximum from Blake Ridge sediments. Earth Planet. Sci. Lett. 266, 61–77.
Haley, B.A., Klinkhammer, G.P., McManus, J., 2004. Rare earth elements in pore waters of marine sediments. Geochim. Cosmochim. Acta 68, 1265–1279.
Haley, B.A., Du, J., Abbott, A.N., Mcmanus, J., 2017. The Impact of Benthic Processes on Rare Earth Element and Neodymium Isotope Distributions in the Oceans. Front. Mar. Sci. 4, 1–12.
Hannigan, R.E., Sholkovitz, E.R., 2001. The development of middle rare earth element enrichments in freshwaters: weathering of phosphate minerals. Chem. Geol. 175, 495–508.
Hatje, V., Bruland, K.W., Flegal, A.R., 2014. Determination of rare earth elements after pre-concentration using NOBIAS-chelate PA-1®resin: Method development and application in the San Francisco Bay plume. Mar. Chem. 160, 34–41.
Heaton, T.J., Köhler, P., Butzin, M., Bard, E., Reimer, R.W., Austin, W.E.N., Bronk, R.C., Grootes, P.M., Hughen, K.A., Kromer, B., Reimer, P.J., Adkins, J., Burke, A., Cook, M.S., Olsen, J., Skinner, L.C., 2020. Marine20 - The Marine Radiocarbon Age Calibration Curve (0–55,000 cal BP). Radiocarbon 62, 779–820.
Hein, J.R., Koschinsky, A., 2014. Deep-Ocean Ferromanganese Crusts and Nodules. Published by Elsevier Inc..
Hillenbrand, C.D., Smith, J.A., Kuhn, G., Esper, O., Gersonde, R., Larter, R.D., Maher, B., Moreton, S.G., Shimmield, T.M., Korte, M., 2010. Age assignment of a diatomaceous ooze deposited in the western Amundsen Sea Embayment after the Last Glacial Maximum. J. Quat. Sci. 25, 280–295.
Hillenbrand, C.D., Smith, J.A., Hodell, D.A., Greaves, M., Poole, C.R., Kender, S., Williams, M., Andersen, T.J., Jernas, P.E., Elderfield, H., Klages, J.P., Roberts, S.J., Gohl, K., Larter, R.D., Kuhn, G., 2017. West Antarctic Ice Sheet retreat driven by Holocene warm water incursions. Nature 547, 43–48.
Holder, L., Duffy, M., Opdyke, B., Leventer, A., Post, A., O'Brien, P., Armand, L.K., 2020. Controls Since the mid - Pleistocene Transition on Sedimentation and Primary Productivity Downslope of Totten Glacier, East Antarctica. Paleoceanogr. Paleoclimatol. 35, 1–25.
Howe, J.N.W., Piotrowski, A.M., Rennie, V.C.F., 2016. Abyssal origin for the early Holocene pulse of unradiogenic neodymium isotopes in Atlantic seawater. Geology 44, 831–834.
Huang, H., Gutjahr, M., Eisenhauer, A., Kuhn, G., 2020. No detectable Weddell Sea Antarctic Bottom Water export during the Last and Penultimate Glacial Maximum. Nat. Commun. 11, 1–10.
Huang, H., Gutjahr, M., Kuhn, G., Hathorne, E.C., Eisenhauer, A., 2021. Efficient Extraction of Past Seawater Pb and Nd Isotope Signatures From Southern Ocean Sediments. Geochem. Geophys. Geosyst. 22, 1–22.
Jacobs, S.S., Hellmer, H.H., Jenkins, A., 1996. Antarctic ice sheet melting in the Southeast Pacific. Geophys. Res. Lett. 23, 957–960.
Jacobsen, S.B., Wasserburg, G.J., 1980. Sm-Nd isotopic evolution of chondrites. Earth Planet. Sci. Lett. 50, 139–155.
Johannesson, K.H., Burdige, D.J., 2007. Balancing the global oceanic neodymium budget: Evaluating the role of groundwater. Earth Planet. Sci. Lett. 253, 129–142.
Kim, M.G., Hyeong, K., Yoo, C.M., 2022. Distribution of Rare Earth Elements and Yttrium in Sediments From the Clarion-Clipperton Fracture Zone, Northeastern Pacific Ocean. Geochem. Geophys. Geosyst., 1–13
Klevenz, V., Vance, D., Schmidt, D.N., Mezger, K., 2008. Neodymium isotopes in benthic foraminifera: Core-top systematics and a down-core record from the Neogene south Atlantic. Earth Planet. Sci. Lett. 265, 571–587.
Kon, Y., Hoshino, M., Sanematsu, K., Morita, S., Tsunematsu, M., Okamoto, N., Yano, N., Tanaka, M., Takagi, T., 2014. Geochemical characteristics of apatite in heavy REE-rich Deep-Sea Mud from Minami-Torishima Area, Southeastern Japan. Resour. Geol. 64, 47–57.
Kraft, S., Frank, M., Hathorne, E.C., Weldeab, S., 2013. Assessment of seawater Nd isotope signatures extracted from foraminiferal shells and authigenic phases of Gulf of Guinea sediments. Geochim. Cosmochim. Acta 121, 414–435.
Lacan, F., Jeandel, C., 2005a. Acquisition of the neodymium isotopic composition of the North Atlantic Deep Water. Geochem. Geophys. Geosyst. 6, 1–20.
Lacan, F., Jeandel, C., 2005b. Neodymium isotopes as a new tool for quantifying exchange fluxes at the continent-ocean interface. Earth Planet. Sci. Lett. 232, 245–257.
Lambelet, M., van de Flierdt, T., Butler, E.C.V., Bowie, A.R., Rintoul, S.R., Watson, R.J., Remenyi, T., Lannuzel, D., Warner, M., Robinson, L.F., Bostock, H.C., Bradtmiller, L.I., 2018. The Neodymium Isotope Fingerprint of Adélie Coast Bottom Water. Geophys. Res. Lett. 45, 11247–11256.
Liao, J., Chen, J., Sun, X., Wu, Z., Deng, Y., Shi, X., Wang, Y., Chen, Y., Koschinsky, A., 2022. Quantifying the controlling mineral phases of rare-earth elements in deep-sea pelagic sediments. Chem. Geol. 595, 1–17.
Lougheed, B.C., Obrochta, S.P., 2016. MatCal : Open Source Bayesian Matlab. J. Open Res. Softw. 4, 1–4.
Lougheed, B.C., Obrochta, S.P., 2019. A Rapid, Deterministic Age-Depth Modeling Routine for Geological Sequences With Inherent Depth Uncertainty. Paleoceanogr. Paleoclimatol. 34, 122–133.
Lumpkin, R., Speer, K., 2007. Global Ocean Meridional Overturning. J. Phys. Oceanogr. 37, 2550–2562.
Maritati, A., Halpin, J.A., Whittaker, J.M., Daczko, N.R., 2019. Fingerprinting Proterozoic Bedrock in Interior Wilkes Land, East Antarctica. Sci. Rep., 1–12
Martin, E.E., Blair, S.W., Kamenov, G.D., Scher, H.D., Bourbon, E., Basak, C., Newkirk, D.N., 2010. Extraction of Nd isotopes from bulk deep sea sediments for paleoceanographic studies on Cenozoic time scales. Chem. Geol. 269, 414–431.

Menviel, L., Timmermann, A., Timm, O.E., Mouchet, A., 2010. Climate and biogeochemical response to a rapid melting of the West Antarctic Ice Sheet during interglacials and implications for future climate. Paleoceanography 25.
Molina-Kescher, M., Frank, M., Hathorne, E.C., 2014. Nd and Sr isotope compositions of different phases of surface sediments in the South Pacific: Extraction of seawater signatures, boundary exchange, and detrital/dust provenance. Geochem. Geophys. Geosyst. 15, 3502–3520.
Möller, A., Post, N.J., Hensen, B.J., 2002. Crustal residence history and garnet Sm-Nd ages of high-grade metamorphic rocks from the Windmill Islands area, East Antarctica. Int. J. Earth Sci. 91, 993–1004.
Moreau, S., Lannuzel, D., Janssens, J., Arroyo, M.C., Corkill, M., Cougnon, E., Genovese, C., Legresy, B., Lenton, A., Puigcorbé, V., Ratnarajah, L., Rintoul, S., Roca-Martí, M., Rosenberg, M., Shadwick, E.H., Silvano, A., Strutton, P.G., Tilbrook, B., 2019. Sea Ice Meltwater and Circumpolar Deep Water Drive Contrasting Productivity in Three Antarctic Polynyas. J. Geophys. Res. Ocean. 124, 2943–2968.
Morlighem, M., Rignot, E., Binder, T., Blankenship, D., Drews, R., Eagles, G., Eisen, O., Ferraccioli, F., Forsberg, R., Fretwell, P., Goel, V., Greenbaum, J.S., Gudmundsson, H., Guo, J., Helm, V., Hofstede, C., Howat, I., Humbert, A., Jokat, W., Karlsson, N.B., Lee, W.S., Matsuoka, K., Millan, R., Mouginot, J., Paden, J., Pattyn, F., Roberts, J., Rosier, S., Ruppel, A., Seroussi, H., Smith, E.C., Steinhage, D., Sun, B., van den Broeke, M.R., van Ommen, T.D., van Wessem, M., Young, D.A., 2020. Deep glacial troughs and stabilizing ridges unveiled beneath the margins of the Antarctic ice sheet. Nat. Geosci. 13, 132–137.
Nieuwenhuize, J., Maas, Y.E.M., Middelburg, J.J., 1994. Rapid analysis of organic carbon and nitrogen in particulate materials. Mar. Chem. 45, 217–224.
O'Nions, R.K., Hamilton, P.J., Evensen, N.M., 1977. Variations in 143Nd/144Nd and 87Sr/86Sr ratios in oceanic basalts. Earth Planet. Sci. Lett. 34, 13–22.
O'Nions, R.K., Carter, S.R., Cohen, R.S., Evensen, N.M., Hamilton, P.J., 1978. Pb, Nd and Sr isotopes in oceanic ferromanganes depostis and ocean floor basalts. Nature 273, 435–438.
Pahnke, K., Goldstein, S.L., Hemming, S.R., 2008. Abrupt changes in antarctic intermediate water circulation over the past 25,000 years. Nat. Geosci. 1, 870–874.
Palmer, M.R., Elderfield, H., 1985. Variations in the Nd isotopic composition of foraminifera from Atlantic Ocean sediments. Earth Planet. Sci. Lett. 73, 299–305.
Pasquier, B., Hines, S.K.V., Liang, H., Wu, Y., Goldstein, S.L., John, S.G., 2022. GNOM v1.0: an optimized steady-state model of the modern marine neodymium cycle. Geosci. Model Dev. 15, 4625–4656.
Patton, G.M., Francois, R., Weis, D., Hathorne, E., Gutjahr, M., Frank, M., Gordon, K., 2021. An experimental investigation of the acquisition of Nd by authigenic phases of marine sediments. Geochim. Cosmochim. Acta 301, 1–29.
Paul, S.A.L., Volz, J.B., Bau, M., Köster, M., Kasten, S., Koschinsky, A., 2019. Calcium phosphate control of REY patterns of siliceous-ooze-rich deep-sea sediments from the central equatorial Pacific. Geochim. Cosmochim. Acta 251, 56–72.
Pérez-Tribouillier, H., Noble, T.L., Townsend, A.T., Bowie, A.R., Chase, Z., 2019. Pre-concentration of thorium and neodymium isotopes using Nobias chelating resin: Method development and application to chromatographic separation. Talanta 202, 600–609.
Piepgras, D.J., Wasserburg, G.J., 1980. Neodymium isotopic variations in seawater. Earth Planet. Sci. Lett. 50, 128–138.
Pin, C., Zalduegui, J.F.S., 1997. Sequential separation of light rare-earth elements, thorium and uranium by miniaturized extraction chromatography: Application to isotopic analyses of silicate rocks. Anal. Chim. Acta 339, 79–89.
Piotrowski, A.M., Goldstein, S.L., Hemming, S.R., Fairbanks, R.G., 2004. Intensification and variability of ocean thermohaline circulation through the last deglaciation. Earth Planet. Sci. Lett. 225, 205–220.
Piotrowski, A.M., Goldstein, S.L., Hemming, S.R., Fairbanks, R.G., 2005. Temporal relationship of carbon cycling and ocean circulation at glacial boundaries. Science (80-.) 307, 1933–1938.
Piotrowski, A.M., Galy, A., Nicholl, J.A.L., Roberts, N., Wilson, D.J., Clegg, J.A., Yu, J., 2012. Reconstructing deglacial North and South Atlantic deep water sourcing using foraminiferal Nd isotopes. Earth Planet. Sci. Lett. 357–358, 289–297.
Pöppelmeier, F., Gutjahr, M., Blaser, P., Keigwin, L.D., Lippold, J., 2018. Origin of Abyssal NW Atlantic Water Masses Since the Last Glacial Maximum. Paleoceanogr. Paleoclimatol. 33, 530–543.
Pöppelmeier, F., Blaser, P., Gutjahr, M., Jaccard, S.L., Frank, M., Max, L., Lippold, J., 2020a. Northern-sourced water dominated the Atlantic Ocean during the Last Glacial Maximum. Geology 48, 826–829.
Pöppelmeier, F., Lippold, J., Blaser, P., Gutjahr, M., Frank, M., Stocker, T.F., 2022. Neodymium isotopes as a paleo-water mass tracer: A model-data reassessment. Quat. Sci. Rev. 279, 107404.
Pöppelmeier, F., Scheen, J., Blaser, P., Lippold, J., Gutjahr, M., Stocker, T.F., 2020b. Influence of Elevated Nd Fluxes on the Northern Nd Isotope End Member of the Atlantic During the Early Holocene. Paleoceanogr. Paleoclimatol. 35.
Rempfer, J., Stocker, T.F., Joos, F., Dutay, J., Siddall, M., 2011. Modelling Nd-isotopes with a coarse resolution ocean circulation model: Sensitivities to model parameters and source/sink distributions. Geochim. Cosmochim. Acta 75, 5927–5950.
Ren, J., Jiang, X., He, G., Wang, F., Yang, T., Luo, S., Deng, Y., Zhou, J., Deng, X., Yao, H., Yu, H., 2022. Enrichment and sources of REY in phosphate fractions: Constraints from the leaching of REY-rich deep-sea sediments. Geochim. Cosmochim. Acta 335, 155–168.
Roberts, N.L., Piotrowski, A.M., Mcmanus, J.F., Keigwin, L.D., 2010. Synchronous Deglacial Overturning and Water Mass Source Changes. Science 80-.). 327, 75–78.
Rousseau, T.C.C., Sonke, J.E., Chmeleff, J., Van Beek, P., Souhaut, M., Boaventura, G., Seyler, P., Jeandel, C., 2015. Rapid neodymium release to marine waters from lithogenic sediments in the Amazon estuary. Nat. Commun. 6.
Rutberg, R.L., Hemming, S.R., Goldstein, S.L., 2000. Reduced North Atlantic Deep Water flux to the glacial Southern Ocean inferred from neodymium isotope ratios. Nature 405, 935–938.
Ruttenberg, K.C., 1992. Development of a sequential extraction method for different forms of phosphorus in marine sediments. Limnol. Oceanogr. 37, 1460–1482.
Ruttenberg, K.C., Berner, R.A., 1993. Authigenic apatite formation and burial in sediments from non-upwelling, continental margin environments. Geochim. Cosmochim. Acta 57, 991–1007.
Sanchez, G., Halpin, J.A., Gard, M., Hasterok, D., Stål, T., Raimondo, T., Peters, S., Burton-Johnson, A., 2021. PetroChron Antarctica: A Geological Database for Interdisciplinary Use. Geochem. Geophys. Geosyst. 22.
Sanchez-Cabeza, J.A., Masqué, P., Ani-Ragolta, I., 1998. 210Pb and 210Po analysis in sediments and soils by microwave acid digestion. J. Radioanal. Nucl. Chem. 227, 19–22.
Scambos, T.A., Bohlander, J.A., Shuman, C.A., Skvarca, P., 2004. Glacier acceleration and thinning after ice shelf collapse in the Larsen B embayment, Antarctica. Geophys. Res. Lett. 31, 2001–2004.
Scher, H.D., Martin, E.E., 2004. Circulation in the Southern Ocean during the Paleogene inferred from neodymium isotopes. Earth Planet. Sci. Lett. 228, 391–405.
Schijf, J., Christenson, E.A., Byrne, R.H., 2015. YREE scavenging in seawater: A new look at an old model. Mar. Chem. 177, 460–471.
Sholkovitz, E.R., Landing, W.M., Lewis, B.L., 1994. Ocean particle chemistry: The fractionation of rare earth elements between suspended particles and seawater. Geochim. Cosmochim. Acta 58, 1567–1579.
Siddall, M., Khatiwala, S., van de Flierdt, T., Jones, K., Goldstein, S.L., Hemming, S., Anderson, R.F., 2008. Towards explaining the Nd paradox using reversible scavenging in an ocean general circulation model. Earth Planet. Sci. Lett. 274, 448–461.
Silvano, A., Rintoul, S.R., Pena-Molino, B., Williams, G.D., 2017. Distribution of water masses and meltwater on the continental shelf near the Totten and Moscow University ice shelves. J. Geophys. Res. Ocean 122, 2050–2068.
Skinner, L.C., Scrivner, A.E., Vance, D., Barker, S., Fallon, S., Waelbroeck, C., 2013. North Atlantic versus southern ocean contributions to a deglacial surge in deep ocean ventilation. Geology 41, 667–670.
Staudigel, H., Doyle, P., Zindler, A., 1985. Sr and Nd isotope systematics in fish teeth. Earth Planet. Sci. Lett. 76, 45–56.
Struve, T., Van De Flierdt, T., Robinson, L.F., Bradtmiller, L.I., Hines, S.K., Adkins, J.F., Lambelet, M., Crocket, K.C., Kreissig, K., Coles, B., Auro, M.E., 2016. Neodymium isotope analyses after combined extraction of actinide and lanthanide elements from seawater and deep-sea coral aragonite. Geochem. Geophys. Geosyst. 17, 232–240.
Struve, T., van de Flierdt, T., Burke, A., Robinson, L.F., Hammond, S.J., Crocket, K.C., Bradtmiller, L.I., Auro, M.E., Mohamed, K.J., White, N.J., 2017. Neodymium isotopes and concentrations in aragonitic scleractinian cold-water coral skeletons - Modern calibration and evaluation of palaeo-applications. Chem. Geol. 453, 146–168.
Tachikawa, K., Athias, V., Jeandel, C., 2003. Neodymium budget in the Modern Ocean and paleo-oceanographic implications. J. Geophys. Res. 108, 1–13.
Takahashi, Y., Hayasaka, Y., Morita, K., Kashiwabara, T., Nakada, R., Marcus, M.A., Kato, K., Tanaka, K., Shimizu, H., 2015. Transfer of rare earth elements (REE) from manganese oxides to phosphates during early diagenesis in pelagic sediments inferred from REE patterns, X-ray absorption spectroscopy, and chemical leaching method. Geochem. J. 49, 653–674.
Tanaka, T., Togashi, S., Kamioka, H., Amakawa, H., Kagami, H., Hamamoto, T., Yuhara, M., Orihashi, Y., Yoneda, S., Shimizu, H., Kunimaru, T., Takahashi, K., Yanagi, T., Nakano, T., Fujimaki, H., Shinjo, R., Asahara, Y., Tanimizu, M., Dragusanu, C., 2000. JNdi-1: A neodymium isotopic reference in consistency with LaJolla neodymium. Chem. Geol. 168, 279–281.
Taylor, S., McLennan, S., 1985. The continental crust: its composition and evolution.
Toyoda, K., Nakamua, Y., Masuda, A., 1990. Rare earth elements of Pacific pelagic sediments. Geochemica Cosmochim. 54, 1093–1103.
Toyoda, K., Tokonami, M., 1990. Diffusion of rare-earth elements in fish teeth from deep-sea sediments. Nature 345, 607–609.
Trotter, J.A., Barnes, C.R., McCracken, A.D., 2016. Rare earth elements in conodont apatite: Seawater or pore-water signatures? Palaeogeogr. Palaeoclimatol. Palaeoecol. 462, 92–100.
van de Flierdt, T., Frank, M., Lee, D.C., Halliday, A.N., Reynolds, B.C., Hein, J.R., 2004. New constraints on the sources and behavior of neodymium and hafnium in seawater from Pacific Ocean ferromanganese crusts. Geochim. Cosmochim. Acta 68, 3827–3843.
van de Flierdt, T., Pahnke, K., Amakawa, H., Andersson, P., Basak, C., Coles, B., Colin, C., Crocket, K., Frank, M., Frank, N., Goldstein, S.L., Goswami, V., Haley, B.A., Hathorne, E.C., Hemming, S.R., Henderson, G.M., Jeandel, C., Jones, K., Kreissig, K., Lacan, F., Lambelet, M., Martin, E.E., Newkirk, D.R., Obata, H., Pena, L., Piotrowski, A.M., Pradoux, C., Scher, H.D., Schöberg, H., Singh, S.K., Stichel, T., Tazoe, H., Vance, D., Yang, J., Gideon, M., Jeandel, C., Jones, K., Kreissig, K., Lacan, F., Lambelet, M., Ellen, E., Newkirk, D.R., Obata, H., Pena, L., Piotrowski, A.M., Pradoux, C., Scher, D., Singh, S.K., Stichel, T., Tazoe, H., Vance, D., Yang, J., 2012. GEOTRACES intercalibration of neodymium isotopes and rare earth element concentrations in seawater and suspended particles. Part 1: reproducibility of results for the international intercomparison. Limnol. Oceanogr. Methods 10, 234–251.

Vance, D., Burton, K., 1999. Neodymium isotopes in planktonic foraminifera: A record of the response of continental weathering and ocean circulation rates to climate change. Earth Planet. Sci. Lett. 173, 365–379.
Wang, R., Williams, T.J., Hillenbrand, C.-D., Ehrmann, W., Larkin, C.S., Hutchings, A. M., Piotrowski, A.M., 2022. Boundary processes and neodymium cycling along the Pacific margin of West Antarctica. Geochim. Cosmochim. Acta 327, 1–20.
Williams, T.J., Martin, E.E., Sikes, E., Starr, A., Umling, N.E., Glaubke, R., 2021. Neodymium isotope evidence for coupled Southern Ocean circulation and Antarctic climate throughout the last 118,000 years. Quat. Sci. Rev. 260, 106915.
Wilson, D.J., Piotrowski, A.M., Galy, A., Clegg, J.A., 2013. Reactivity of neodymium carriers in deep sea sediments: Implications for boundary exchange and paleoceanography. Geochim. Cosmochim. Acta 109, 197–221.
Wilson, D.J., Crocket, K.C., Van De Flierdt, T., Robinson, L.F., Adkins, J.F., 2015. Dynamic intermediate ocean circulation in the North Atlantic during Heinrich Stadial 1: A radiocarbon and neodymium isotope perspective. Paleoceanography 29, 1072–1093.
Wilson, D.J., Bertram, R.A., Needham, E.F., van de Flierdt, T., Welsh, K.J., McKay, R.M., Mazumder, A., Riesselman, C.R., Jimenez-Espejo, F.J., Escutia, C., 2018. Ice loss from the East Antarctic Ice Sheet during late Pleistocene interglacials. Nature 561, 383.
Wu, Q., Colin, C., Liu, Z., Thil, F., Dubois-Dauphin, Q., Frank, N., Tachikawa, K., Bordier, L., Douville, E., 2015. Neodymium isotopic composition in foraminifera and authigenic phases of the South China Sea sediments: Implications for the hydrology of the North Pacific Ocean over the past 25 kyr Qiong. Geochem. Geophys. Geosyst. 16, 3883–3904.
Yasukawa, K., Liu, H., Fujinaga, K., Machida, S., Haraguchi, S., 2014. Geochemistry and mineralogy of REY-rich mud in the eastern Indian Ocean. J. Asian Earth Sci. 93, 25–36.
Zhang, S.H., Zhao, Y., Liu, X.C., Liu, Y.S., Hou, K.J., Li, C.F., Ye, H., 2012. U-Pb geochronology and geochemistry of the bedrocks and moraine sediments from the Windmill Islands: Implications for Proterozoic evolution of East Antarctica. Precambrian Res. 206–207, 52–71.